nature geoscience

ARTICLES

https://doi.org/10.1038/s41561-022-00998-z

Check for updates

Sill-controlled salinity contrasts followed post-Messinian flooding of the Mediterranean

Udara Amarathunga[1]✉, Andrew McC. Hogg[1], Eelco J. Rohling[1,2], Andrew P. Roberts[1], Katharine M. Grant[1], David Heslop[1], Pengxiang Hu[1], Diederik Liebrand[3,5], Thomas Westerhold[3], Xiang Zhao[1] and Stewart Gilmore[4]

A mile-high marine cascade terminated the Messinian salinity crisis 5.33 Myr ago, due to partial collapse of the Gibraltar sill that had isolated a largely desiccated Mediterranean from the Atlantic Ocean. Atlantic waters may have refilled the basin within 2 years. Prevailing hypotheses suggest that normal marine conditions were established across the Mediterranean immediately after the catastrophic flooding. Here we use proxy data and fluid physics-based modelling to show that normal conditions were likely for the western Mediterranean, but that flooding caused a massive transfer of salt from the western to the eastern Mediterranean across the Sicily sill, which became a hyper-salinity-stratified basin. Hyper-stratification inhibited deep-water ventilation, causing anomalously long-lasting organic-rich (sapropel) sediment deposition. Model data agreement indicates that hyper-stratification breakdown by diapycnal diffusion required 26,000 years. An alternative hypothesis that Atlantic reconnection occurred after the Mediterranean had largely been refilled is inconsistent with our observations, as this would have led to hyper-stratification and sapropel formation in both basins. Our findings offer insight into the role of stratification in delaying the re-establishment of normal marine conditions following abrupt refilling of a previously desiccated ocean basin.

The 630,000-year Messinian salinity crisis (MSC) resulted from progressive closure of the connection(s) between the Mediterranean Sea and Atlantic Ocean ~5.96 Myr ago (Ma)[1–3]. During the MSC, massive evaporite sequences were deposited. A phase of kilometre-scale Mediterranean drawdown occurred[4], resulting in a basin-wide Messinian erosional surface[5], and 2,500 m and 1,300 m deep Messinian canyons excavated beneath the Nile delta and the Rhône River mouth, respectively[6,7]. It has long been inferred that Mediterranean sea levels were low, ~1,300 m to ~2,700 m below global sea level[5,8–11], prior to the earliest Pliocene (Zanclean) megaflood event that terminated the MSC. Alternatively, geochemical and palaeobiological evidence from latest Messinian evaporites may imply elevated basin levels, attributing the drawdown to an older Messinian phase[12]. In that scenario, increased Paratethyan and occasional Atlantic inflows are suggested to have largely refilled the Mediterranean[13] (a shallow Mediterranean base level below Atlantic, with interconnected sub-basins) with lower-salinity water overlying deep hypersaline fluids prior to complete Atlantic reconnection[12–14]. We investigate the consequences of abrupt refilling of a partially desiccated basin (a kilometre-scale drawdown in the megaflood hypothesis) and address the alternative hypothesis in a sensitivity test (see Methods and Extended Data Figs. 6–8).

Evidence supporting the megaflood hypothesis

The megaflood hypothesis is based on seismic and borehole data from both the western and eastern Mediterranean (wMed and eMed, respectively)[15–17]. Critical evidence at the Strait of Gibraltar comes from a massive erosive channel in the Gibraltar arc/sill, which extends 390 km from the Gulf of Cadiz on the Atlantic side towards the deep Alboran Sea on the Mediterranean side; the so-called Zanclean channel[3]. Elongated megabar deposits detected alongside the main erosive channel in the eastern Alboran Sea have been related to the flooding event[16]. This sharply defined channel has maximum depth and width of 650 m and 15 km, respectively[3,16]. The dimensions of this incision have led to model estimates of water fluxes of up to ~150 Sverdrups (Sv, 1 ×10^6 m^3 s^{-1}) during the Zanclean flood[3].

The most plausible floodwater passage from the wMed into the eMed is the Noto Canyon, which was carved into the Malta escarpment[15,16]. Upslope, this canyon comprises a 400-m-deep and 4-km-wide erosive channel, with Pliocene–Quaternary sediment infill[15]. At the Noto Canyon outlet, seismic stratigraphy in the western Ionian basin reveals a buried chaotic sediment body that extends over an area of 11,000 km^2 and reaches a volume of 1,430–1,620 km^3 (refs. [15,16]). This unit has been interpreted as a megaflood deposit of material that was eroded, transported and deposited during a catastrophic flooding event at the Miocene/Pliocene (M/P) transition[15,16].

The M/P boundary was drilled at several Deep Sea Drilling Project (DSDP) and Ocean Drilling Program (ODP) sites in the deep Mediterranean[18]. It is characterized by a sharp lithological change, which has been attributed to an abrupt return to open-marine conditions across the Mediterranean, terminating the MSC[16,18,19]. However, where continuous records across the boundary are available, a major difference can be seen between Mediterranean sub-basins (Supplementary Table 1 and Extended Data Fig. 1). In the wMed, complete records across the M/P transition from the Tyrrhenian Sea, Balearic margin and Alboran Sea (Supplementary Table 1) reveal earliest Pliocene foraminifera-nannofossil oozes over late Messinian evaporative sequences. This sequence suggests that normal marine conditions were established rapidly in the wMed following flooding (Supplementary Table 1). In contrast, eMed cores

[1]Research School of Earth Sciences, Australian National University, Canberra, Australian Capital Territory, Australia. [2]Ocean and Earth Science, University of Southampton, National Oceanography Centre, Southampton, UK. [3]MARUM, University of Bremen, Bremen, Germany. [4]Geoscience Australia, Canberra, Australian Capital Territory, Australia. [5]Present address: PalaeoClimate.Science, Allerton Bywater, UK. ✉e-mail: udara.amarathunga@anu.edu.au

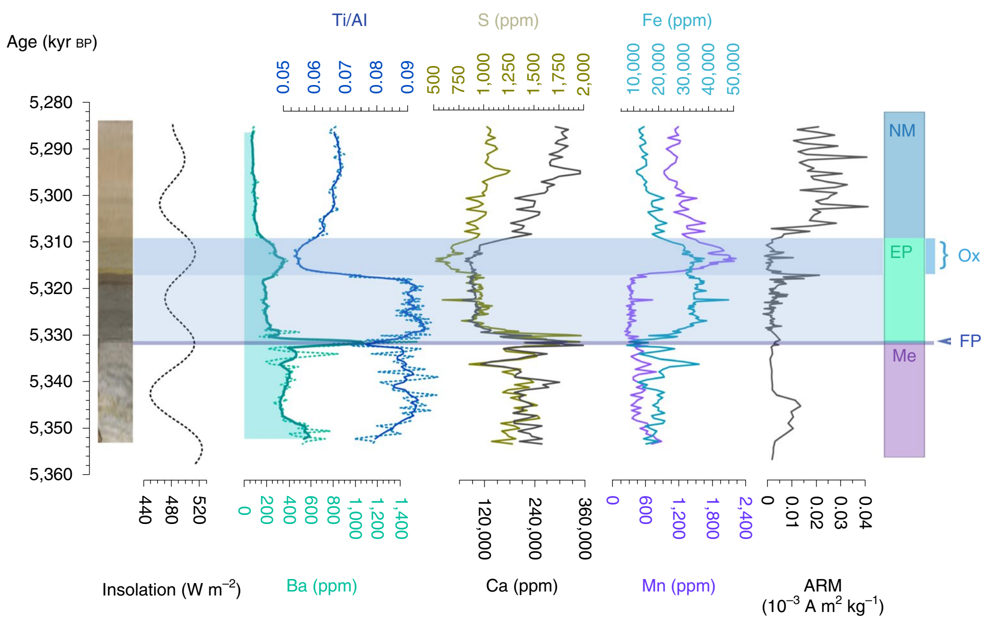

Fig. 1 | XRF core-scanning and magnetic data across the M/P boundary from ODP Site 967. The M/P transition is tuned to the 65° N insolation maximum at 5.333 Ma (see Extended Data Fig. 3). Return to normal marine conditions is marked by a sudden jump in Ca concentration at around 5.307 Ma. Elevated Ba concentrations indicate organic matter preservation between the first two Pliocene insolation maxima (mystery sapropel). The intervening insolation minimum records more than twice as high Ba concentrations compared with normal marine (NM) conditions. For Ba and Ti/Al, dotted lines in the background indicate original XRF data. Thick lines are the five-point moving average of the two records. The upper portion of the mystery sapropel has been oxidized as indicated by Mn, S and ARM profiles (Ox). Me, Messinian; FP, flooding phase (Zanclean flooding surface); EP, evolving phase.

indicate deposition of a thick organic-rich layer (sapropel) in the earliest Pliocene, which was first detected in DSDP Site 376 from the Florence Rise and named the 'mystery sapropel'[20]. ODP Site 969 on the Mediterranean Ridge contains a similarly thick, laminated sapropel immediately above the flooding surface (Supplementary Table 1). Absence of benthic foraminifera in this sapropel indicates a lack of eMed deep-water ventilation/ oxygenation in the immediate flood aftermath, in contrast to better wMed ventilation[20].

More evidence for the mystery sapropel

At eMed ODP Site 967 (Eratosthenes seamount), late Messinian brecciated carbonates (with gypsum[21]) are overlain by dark grey to olive green earliest Pliocene sediments[21,22]. Throughout the sediments younger than ~3.2 Ma at Site 967, colour reflectance records and oxygen isotope stratigraphy indicate a regular pattern of sapropel occurrence, visibly recognizable as dark layers[21,23,24]. Between 3.2 and 5.33 Ma, there are no visible sapropels, but there are red intervals resulting from post-depositional sapropel oxidation[21,23,24] (Extended Data Fig. 2). These red intervals contain similar Ba enrichments as sapropels, which are associated with organic matter burial and remained present even after post-depositional oxygenation[25,26]; thus, Ba enrichment is a reliable proxy for original sapropel extents and for detecting sapropels that were initially present but that were later oxidized[25–28]. Throughout the last ~14 Myr, sapropel deposition (and associated Ba peaks) consistently occurred during high-amplitude precession-driven insolation maxima, where the amplitude is modulated by orbital eccentricity maxima[29,30].

Here we present core-scanning X-ray fluorescence (XRF) and magnetic data across the M/P boundary at ODP Site 967 (Supplementary Information) that corroborate the deposition of an organic-rich layer immediately following the M/P transition (Fig. 1). From our results, this layer comprises two Ba peaks with lower (but still substantially elevated) Ba levels in-between (Fig. 1). This Ba pattern is mirrored by two Ti/Al minima with an intervening maximum (Fig. 1). In the eMed sapropel stratigraphy, these mirrored fluctuations are typical of two insolation maxima with an intervening minimum[31–33]. Our chronology suggests that this organic-rich sediment deposition persisted over a 26,000-year period (Extended Data Fig. 3 and Supplementary Table 2). Profiles of redox-sensitive elements and anhysteretic remanent magnetization (ARM) across the organic-rich layer (Fig. 1) are also typical of sapropels[25,26,28]. This 26,000-year interval represents the only Neogene example of a sapropel that extends through an insolation minimum; it breaks the well-understood relationship between sapropel deposition and African monsoon maxima associated with Northern Hemisphere insolation maxima[29,34–37]. In this conventional mode, monsoon maxima caused extensive freshwater flooding into the Mediterranean[36,38–40], which drove both enhanced stratification (curtailing new deep-water ventilation/oxygenation) and enhanced organic export production[29,41,42]. Meanwhile, the monsoon maximum suppressed wind transport of Ti-rich dust to the eMed[26,31,43]. Extension of the sapropel at the M/P boundary across an African monsoon minimum (insolation minimum) is a clear indication of the operation of an additional mechanism that was unique to this event with respect to the entire Neogene.

Establishment of normal marine conditions

The terminal Messinian was a period of surface dilution that resulted from increased Paratethyan and riverine freshwater input (Lago Mare events), punctuated by local gypsum deposition during times of enhanced evaporation[32,44,45]. In our main scenario, deep Mediterranean basins prior to the Zanclean flooding were filled with residual high-salinity brines that in places exceeded 2 km in thickness[9,32,44]. Here, we consider 'late Messinian brines' to have been derived from MSC Stage 2 fluid dilution (when halite precipitated in the wMed and eMed[45]), including potential contributions from halite re-dissolution. We set the brine concentration to 140 practical salinity units (PSU; see Methods for explanation on choice of brine salinity). A qualitative conceptual refill scenario can then be formulated based on energy- and mass-balance arguments (the alternative

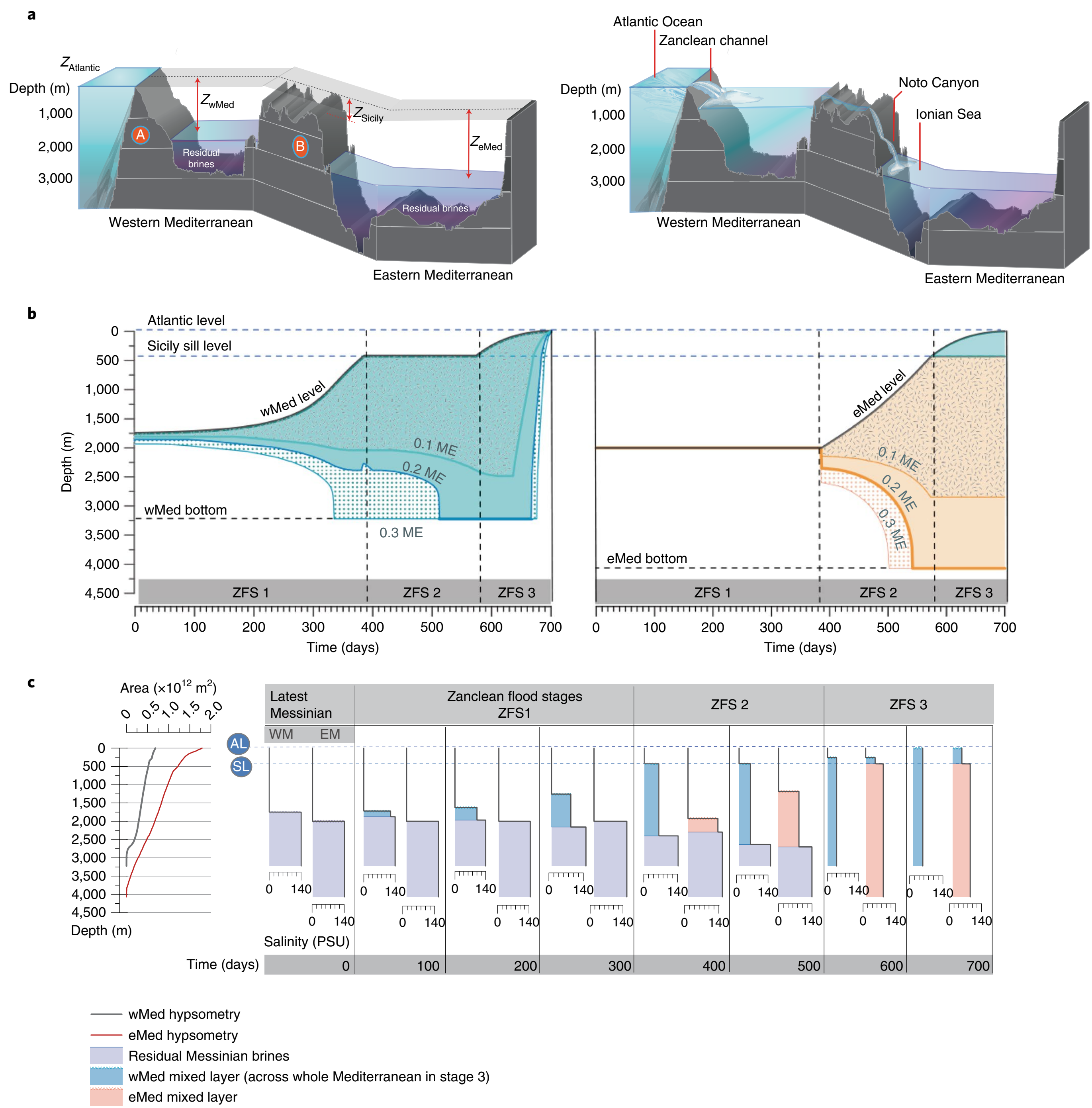

Fig. 2 | Evolution of Mediterranean sub-basins during the Zanclean flood. **a**, Sketches of the basin configuration during the latest Messinian (left) and flooding phase (right). A, Camarinal sill; B, Sicily sill; Z_{wMed}/Z_{eMed}, Messinian drawdown in wMed/eMed; Z_{Sicily}, depth to Sicily sill; $Z_{Atlantic}$, Atlantic Sea surface. **b**, Mixed-layer evolution with time for western and eastern basins. Thick black line indicates sea-level rise in both basins with time (wMed and eMed levels). Coloured, hatched and dotted backgrounds indicate the mixing extent at mixing efficiency (ME) = 0.2, 0.1 and 0.3, respectively. The difference between the basin level curve and the mixed-layer curve gives the mixed-layer thickness at a given time. **c**, Reconstructed wMed and eMed hypsometry (left), and salinity profile evolution (right) for wMed and eMed at each 100-day interval. Salinity profiles (thick black lines) are given in PSU (from 0 to 140 in each diagram). ZFS 1 terminates as the wMed level reaches the Sicily sill; ZFS 2 terminates as eMed level reaches the Sicily sill; during ZFS 3 both basins rise to the Atlantic level simultaneously. ZFS, Zanclean flood stage; AL, Atlantic level; SL, Sicily sill level; WM, western Mediterranean; EM, eastern Mediterranean.

hypothesis starting with a largely refilled late Messinian basin[12–14] is addressed in a sensitivity test; see Methods). In the main scenario, the high-energy Atlantic floodwater cascading into a partially desiccated Mediterranean would have encountered and vigorously mixed with residual wMed brines, while the wMed filled to the height of the sill in the Strait of Sicily (Extended Data Fig. 4). Mixed wMed brine would then have broken through and cut the Noto Canyon, cascading into the eMed. Meanwhile, wMed sea level would have

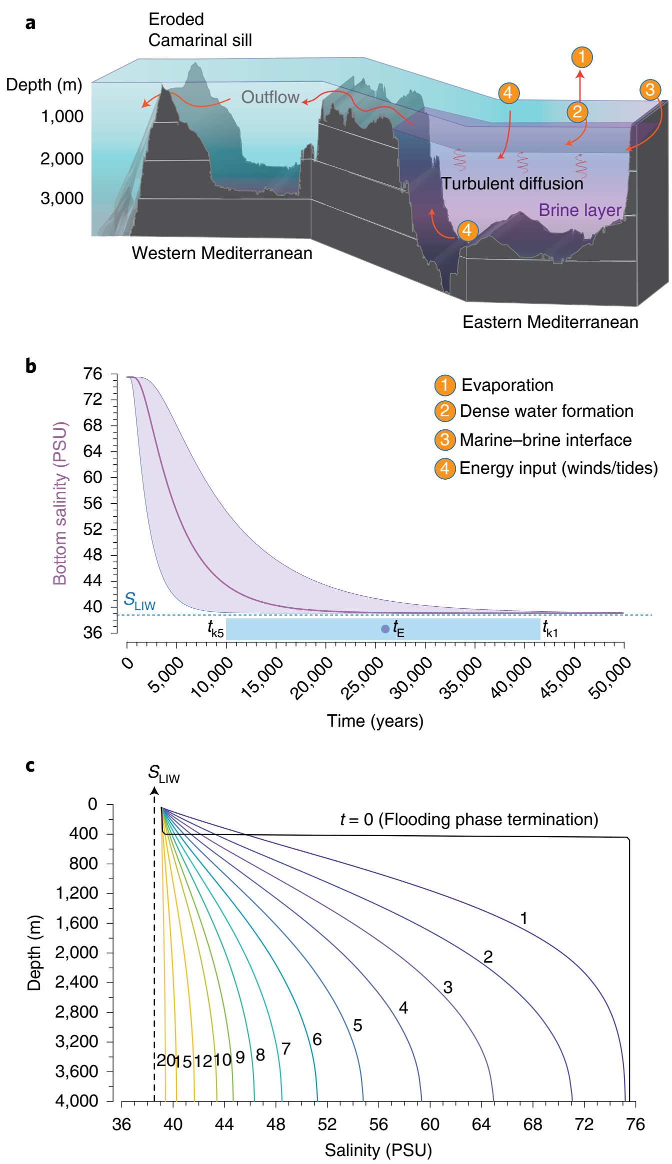

Fig. 3 | Mediterranean evolution during the evolving phase. a, A sketch of the main processes involved in brine removal from the eMed during the evolving phase. Here, the eMed brine layer formed at the end of the flooding phase, as a result of wMed salt transfer and mixing with eMed residual Messinian brines. This layer should not be confused with 'residual Messinian brines' that existed before the flood. **b**, Bottom salinity evolution with time. The thick line is the salinity evolution for diapycnal diffusivity $K_S = 2 \times 10^{-5}$ m^2 s^{-1}. Upper and lower envelopes mark the evolution at diffusivities of 1×10^{-5} m^2 s^{-1} and 5×10^{-5} m^2 s^{-1}, respectively. t_{k1} and t_{k5} are the durations taken to erode the brine at 1×10^{-5} m^2 s^{-1} and 5×10^{-5} m^2 s^{-1}, respectively. The time window between t_{k1} and t_{k5} demarcates all possible time frames within mentioned diffusivity values. t_E is the duration recorded by proxy data (26,000 years). S_{LIW}, Levantine intermediate water salinity. **c**, Evolution of eMed salinity profile with time for $K_S = 2 \times 10^{-5}$ m^2 s^{-1}. Numbers on each curve represent time evolved in thousand years (1 = 1,000 years and so on).

remained several hundred metres below Atlantic sea level, which continued the Atlantic cascade through the Zanclean channel, mixing with wMed brines. Thus, we expect massive salt transfer from the steadily diluting wMed into the filling eMed. Once eMed and wMed sea levels equalized, the level across both basins would have risen in unison, until it equalized with Atlantic sea level across the Strait of Gibraltar. Approximately balanced Atlantic inflow and Mediterranean outflow then drove gradual excess salt removal from the Mediterranean. At this stage, stratification was much less pronounced in the wMed than in the eMed because of the prior wMed salt transfer into the eMed (as the latter filled). Inhibition of deep-water ventilation during this hyper-stratified brine-filled eMed period—accentuated by monsoon flooding during insolation maxima—may then explain the anomalously long duration of the 'mystery sapropel' spanning two insolation maxima and an intervening minimum.

Our qualitative concept requires quantitative assessment, especially to evaluate whether the hypothesized mixing processes are realistic energetically and whether (and why) eMed stratification persisted for ~26,000 years, as derived from our XRF-based sapropel stratigraphy and insolation tuning (see Methods and Extended Data Fig. 3). For this purpose, we present a brine evolution model for the flooding event and its aftermath. Our model considers post-Messinian Mediterranean basin evolution in two successive phases: (1) the flooding phase and (2) an evolving phase. The switch between phases occurred when Mediterranean sea level matched Atlantic sea level across the Strait of Gibraltar.

The flooding phase is characterized by release of enormous gravitational potential energy. This potential energy is converted to kinetic energy as Atlantic floodwaters cascade into the wMed, which we estimate may have exceeded 1.6×10^{19} J d^{-1} at peak flood (Supplementary Fig. 1), or more than 500 times the kinetic energy dissipation at Niagara Falls in one year[46]. This energy is sufficient to mix (most of) the existing wMed brines with Atlantic inflow, forming a deep mixed layer atop potential residual brine (Fig. 2 and Methods). As the rising wMed sea level reached the crest of the Sicily sill, mixed wMed waters started cascading into the eMed via Noto Canyon. Given a smaller channel cross-section in Noto Canyon than in the Zanclean channel, we find that an even more energetic flow entered the eMed than the wMed (Supplementary Fig. 1). Note that our method calculates the minimum flow, restricted only by channel dimensions, and that more energy would have been available in reality because of the steep drop in this passage[15,16]. A massive amount of wMed mixed brine was transferred into the eMed through Noto Canyon because the eMed volume is ~2.5 times greater than the wMed, while—at the same time—Atlantic inflow through the Zanclean channel continued to dilute the wMed mixed layer. We find that >95% of the wMed excess salt ended up in the eMed, as this basin filled (Fig. 2). Once eMed sea level reached the Sicily sill, energy transfer across the sill diminished as the cascade terminated gradually. Later, while both basin levels rose together to the Atlantic level, enhanced mixing occurred only in the vicinity of the Gibraltar sill, further diluting the western basin (Fig. 2 and Extended Data Figs. 4 and 5).

At the flooding phase conclusion, dense (post-flood) brines had filled the eMed to the Sicily sill. For the Mediterranean to return to normal marine conditions, the salt in this brine must have been transferred out of the basin, into the Atlantic Ocean. Eroding the deep brine layer required mixing across the interface separating the brine from shallower, inflow-dominated lower-salinity waters. This mixing would have been governed by similar processes to those operating in the modern global ocean: diapycnal mixing due to wind forcing, tidal interaction with bathymetry and internal wave breaking[47]. These processes lead to estimated diapycnal diffusivity values within a 1–5 $\times 10^{-5}$ m^2 s^{-1} range[48]; we use this range to estimate mixing timescales and their uncertainties. The wide uncertainty range used here is derived from the competing effects of mixing inhibition owing to stronger stratification and enhanced mixing within a smaller basin (with greater boundary interactions).

We model the evolving phase using diapycnal diffusivity in the stated range to remove salt by mixing. We obtain timescales of 10,000–40,000 years (Fig. 3b). The ~26,000-year duration estimated from our proxy data agrees well with this range and corresponds to a diapycnal diffusivity of 2×10^{-5} m^2 s^{-1}. We calculate that this process would have released more than 7×10^{16}kg of excess salt into the Atlantic Ocean within that time period, via Mediterranean outflow. Eventually, salt removal from the deeper eMed reduced stratification sufficiently to allow winter-cooled surface waters to attain densities conducive to new deep-water formation. This facilitated restart of deep-water ventilation and oxygenation, which ended the evolving phase marked by the 'mystery sapropel'. Downward oxidation of reduced sapropel sediments under an oxygenated water column caused a 'burn down' oxidation front in the upper 35 cm of the sapropel[26–28,49,50] (Fig. 1).

We propose that absence of a wMed sapropel following the flooding resulted from wMed brine transfer to the eMed during a high-energy mixing and refilling episode. Our sensitivity test evaluates an alternative ending to the MSC, starting with a deep-water column of residual brine overlain by lower-salinity brackish waters that had refilled the basin before Atlantic reconnection[12–14]. We find that there is insufficient energy in this scenario to remove brine from the wMed (Extended Data Figs. 6–8 and Methods), and a long phase of anoxic (sapropel) deposition would be expected in both the wMed and eMed, which conflicts with available observations (Supplementary Table 1). This offers strong support for a partially desiccated Mediterranean state prior to Atlantic reconnection. To account for potential post-Messinian tectonic movements that may have affected the Sicily sill depth[9,14], and to test for the minimum wMed and eMed base level drops below Atlantic level required to validate our hypothesis, we perform additional sensitivity tests (Methods). Results of the analysis support available observations, further strengthening our hypothesis (Extended Data Figs. 9 and 10).

We find that only a kilometre-scale base level fall in both basins at the terminal Messinian would have resulted in the observed proxy records and modelling outcomes. We conclude that the transition from a partially desiccated Mediterranean basin to normal marine conditions was much less rapid than basin refilling; the full transition took ~26,000 years, whereas flooding/refilling took only ~2 years (Figs. 2 and 3). The ~26,000-year timescale is corroborated quantitatively by our model, which suggests that a 10,000–40,000-year duration is expected. Throughout this time, hyper-stratified eMed conditions caused persistence of an anomalously long interval of organic-rich sediment deposition that extended through two precession-related insolation maxima and the intervening minimum.

Online content

Any methods, additional references, Nature Research reporting summaries, source data, extended data, supplementary information, acknowledgements, peer review information; details of author contributions and competing interests; and statements of data and code availability are available at https://doi.org/10.1038/s41561-022-00998-z.

Received: 12 May 2021; Accepted: 29 June 2022;
Published online: 11 August 2022

References

1. Krijgsman, W., Hilgen, F. J., Raffi, I., Sierro, F. J. & Wilson, D. S. Chronology, causes and progression of the Messinian salinity crisis. *Nature* **400**, 652–655 (1999).
2. Manzi, V. et al. Age refinement of the Messinian salinity crisis onset in the Mediterranean. *Terra Nova* **25**, 315–322 (2013).
3. Garcia-Castellanos, D. et al. Catastrophic flood of the Mediterranean after the Messinian salinity crisis. *Nature* **462**, 778–781 (2009).
4. Hsü, K. J., Ryan, W. B. F. & Cita, M. B. Late Miocene desiccation of the Mediterranean. *Nature* **242**, 240–244 (1973).
5. Urgeles, R. et al. New constraints on the Messinian sealevel drawdown from 3D seismic data of the Ebro margin, western Mediterranean. *Basin Res.* **23**, 123–145 (2011).
6. Barber, P. M. Messinian subaerial erosion of the proto-Nile delta. *Mar. Geol.* **44**, 253–272 (1981).
7. Clauzon, G. Le canyon messinien du Rhone: une preuve decisive du 'desiccated deep-basin model' (Hsu, Cita et Ryan 1973). *Bull. Soc. Geol. Fr.* https://doi.org/10.2113/gssgfbull.s7-xxiv.3.597 (1982).
8. Gargani, J. & Rigollet, C. Mediterranean Sea level variations during the Messinian salinity crisis. *Geophys. Res. Lett.* **34**, L10405 (2007).
9. Blanc, P. L. Improved modelling of the Messinian salinity crisis and conceptual implications. *Palaeogeogr. Palaeoclimatol. Palaeoecol.* **238**, 349–372 (2006).
10. Meijer, P. T. & Krijgsman, W. A quantitative analysis of the desiccation and re-filling of the Mediterranean during the Messinian salinity crisis. *Earth Planet. Sci. Lett.* **240**, 510–520 (2005).
11. Blanc, P. L. The opening of the Plio-Quaternary Gibraltar Strait: assessing the size of a cataclysm. *Geodin. Acta* **15**, 303–317 (2002).
12. García-Veigas, J., Cendón, D. I., Gibert, L., Lowenstein, T. K. & Artiaga, D. Geochemical indicators in western Mediterranean Messinian evaporites: implications for the salinity crisis. *Mar. Geol.* **403**, 197–214 (2018).
13. Marzocchi, A., Flecker, R., van Baak, C. G. C., Lunt, D. J. & Krijgsman, W. Mediterranean outflow pump: an alternative mechanism for the Lago-Mare and the end of the Messinian salinity crisis. *Geology* **44**, 523–526 (2016).
14. Andreetto, F. et al. Freshening of the Mediterranean salt giant: controversies and certainties around the terminal (Upper Gypsum and Lago-Mare) phases of the Messinian salinity crisis. *Earth-Sci. Rev.* **216**, 103577 (2021).
15. Micallef, A. et al. Evidence of the Zanclean megaflood in the eastern Mediterranean basin. *Sci. Rep.* **8**, 1078 (2018).
16. Garcia-Castellanos, D. et al. The Zanclean megaflood of the Mediterranean – searching for independent evidence. *Earth-Sci. Rev.* **201**, 103061 (2020).
17. Camerlenghi, A. et al. Seismic markers of the Messinian salinity crisis in the deep Ionian basin. *Basin Res.* **32**, 716–738 (2020).
18. Pierre, C., Rouchy, J. M. & Blanc-Valleron, M. M. Sedimentological and stable isotope changes at the Messinian/Pliocene boundary in the eastern Mediterranean (holes 968A, 969A, and 969B). *Proc. Ocean Drill. Progr. Sci. Results* **160**, 3–8 (1998).
19. Iaccarino, S. M. & Bossio, A. Paleoenvironment of uppermost Messinian sequences in the western Mediterranean (site 974, 975, and 978). *Proc. Ocean Drill. Progr. Sci. Results* **161**, 529–541 (1999).
20. Hsu, K. et al. Messinian Paleoenvironments, initial reports. *Deep Sea Drill. Proj.* **42-1**, 1003–1035 (1978); https://doi.org/10.2973/dsdp.proc.42-1.153.1978
21. Emeis, K., Roberston, A. H. & Richter, C. Site 967, initial reports. *Proc. Ocean Drill. Progr.* **160**, 215–287 (1996).
22. Spezzaferri, S., Cita, M. B. & McKenzie, J. A. The Miocene/Pliocene boundary in the eastern Mediterranean: results from Sites 967 and 969. *Proc. Ocean Drill. Progr. Sci. Results* **160**, 9–28 (1998).
23. Emeis, K. C., Sakamoto, T., Wehausen, R. & Brumsack, H. J. The sapropel record of the eastern Mediterranean Sea - results of Ocean Drilling Program Leg 160. *Palaeogeogr. Palaeoclimatol. Palaeoecol.* **158**, 371–395 (2000).
24. Grant, K. M. et al. Organic carbon burial in Mediterranean sapropels intensified during Green Sahara periods since 3.2 Myr ago. *Commun. Earth Environ.* **3**, 11 (2022).
25. Van Santvoort, P. J. M., De Lange, G. J., Langereis, C. G., Dekkers, M. J. & Paterne, M. Geochemical and paleomagnetic evidence for the occurrence of 'missing' sapropels in eastern Mediterranean sediments. *Paleoceanography* **12**, 773–786 (1997).
26. Larrasoaña, J. C., Roberts, A. P., Hayes, A., Wehausen, R. & Rohling, E. J. Detecting missing beats in the Mediterranean climate rhythm from magnetic identification of oxidized sapropels (Ocean Drilling Program Leg 160). *Phys. Earth Planet. Inter.* **156**, 283–293 (2006).
27. De Lange, G. J. et al. Synchronous basin-wide formation and redox-controlled preservation of a Mediterranean sapropel. *Nat. Geosci.* **1**, 606–610 (2008).
28. Mercone, D., Thomson, J., Abu-Zied, R. H., Croudace, I. W. & Rohling, E. J. High-resolution geochemical and micropalaeontological profiling of the most recent eastern Mediterranean sapropel. *Mar. Geol.* **177**, 25–44 (2001).
29. Rohling, E. J., Marino, G. & Grant, K. M. Mediterranean climate and oceanography, and the periodic development of anoxic events (sapropels). *Earth-Sci. Rev.* **143**, 62–97 (2015).
30. Larrasoaña, J. C., Roberts, A. P. & Rohling, E. J. Dynamics of Green Sahara periods and their role in hominin evolution. *PLoS ONE* **8**, e76514 (2013).
31. Wehausen, R. & Brumsack, H. J. Chemical cycles in Pliocene sapropel-bearing and sapropel-barren eastern Mediterranean sediments. *Palaeogeogr. Palaeoclimatol. Palaeoecol.* **158**, 325–352 (2000).
32. Ryan, W. B. F. Modeling the magnitude and timing of evaporative drawdown during the Messinian salinity crisis. *Stratigraphy* **5**, 227–243 (2008).
33. Lourens, L. J., Wehausen, R. & Brumsack, H. J. Geological constraints on tidal dissipation and dynamical ellipticity of the Earth over the past three million years. *Nature* **409**, 1029–1033 (2001).
34. Hilgen, F. J. Astronomical calibration of Gauss to Matuyama sapropels in the Mediterranean and implication for the Geomagnetic Polarity Time Scale. *Earth Planet. Sci. Lett.* **104**, 226–244 (1991).

35. Lourens, L. J. et al. Evaluation of the Plio-Pleistocene astronomical timescale. *Paleoceanography* **11**, 391–413 (1996).
36. Rossignol-Strick, M., Nesteroff, W., Olive, P. & Vergnaud Grazzini, C. After the deluge: Mediterranean stagnation and sapropel formation. *Nature* **295**, 105–110 (1982).
37. Rossignol-Strick, M. African monsoons, an immediate climate response to orbital insolation. *Nature* **304**, 46–49 (1983).
38. Osborne, A. H. et al. A humid corridor across the Sahara for the migration of early modern humans out of Africa 120,000 years ago. *Proc. Natl Acad. Sci. USA* **105**, 16444–16447 (2008).
39. Amies, J. D., Rohling, E. J., Grant, K. M., Rodríguez-Sanz, L. & Marino, G. Quantification of African monsoon runoff during last interglacial sapropel S5. *Paleoceanogr. Paleoclimatol.* **34**, 1487–1516 (2019).
40. Rohling, E. J. et al. Reconstructing past planktic foraminiferal habitats using stable isotope data: a case history for Mediterranean sapropel S5. *Mar. Micropaleontol.* **50**, 89–123 (2004).
41. Rohling, E. J. & Gieskes, W. W. C. Late Quaternary changes in Mediterranean intermediate water density and formation rate. *Paleoceanography* **4**, 531–545 (1989).
42. Rohling, E. J. Shoaling of the eastern Mediterranean pycnocline due to reduction of excess evaporation: implications for sapropel formation. *Paleoceanography* **6**, 747–753 (1991).
43. Larrasoaña, J. C. et al. Source-to-sink magnetic properties of NE Saharan dust in eastern Mediterranean marine sediments: review and paleoenvironmental implications. *Front. Earth Sci.* **3**, 19 (2015).
44. Rouchy, J. M. & Caruso, A. The Messinian salinity crisis in the Mediterranean basin: a reassessment of the data and an integrated scenario. *Sediment. Geol.* **188–189**, 35–67 (2006).
45. Roveri, M. et al. The Messinian salinity crisis: past and future of a great challenge for marine sciences. *Mar. Geol.* **352**, 25–58 (2014).
46. Hayakawa, Y. S. & Matsukura, Y. Factors influencing the recession rate of Niagara Falls since the 19th century. *Geomorphology* **110**, 212–216 (2009).
47. Ferrari, R. & Wunsch, C. Ocean circulation kinetic energy: reservoirs, sources, and sinks. *Annu. Rev. Fluid Mech.* **41**, 253–282 (2009).
48. Waterhouse, A. F. et al. Global patterns of diapycnal mixing from measurements of the turbulent dissipation rate. *J. Phys. Oceanogr.* **44**, 1854–1872 (2014).
49. Thomson, J. et al. Redistribution and geochemical behaviour of redox-sensitive elements around S1, the most recent eastern Mediterranean sapropel. *Geochim. Cosmochim. Acta* **59**, 3487–3501 (1995).
50. Reitz, A., Thomson, J., Lange, G. J., De & Hensen, C. Source and development of large manganese enrichments above eastern Mediterranean sapropel S1. *Paleoceanography* **21**, PA3007 (2006).

Methods

Bulk sediment geochemistry. We present XRF core-scanner data from ODP Site 967 for the 5.12–5.35 Ma interval. Scanning was performed on archive core sections at MARUM-University of Bremen on an Avaatech XRF core scanner. Core sections were covered with 4-mm-thick Ultralene film and measured at 50 and 30 kV with 0.55 mA current and with a Cu and Pd thick filter, respectively, and at 10 kV with 0.035 mA current (no filter); count time for all runs was 7 s. Element 'counts' for the entire interval were converted into element concentrations by multivariate log-ratio calibration[51], using new wavelength dispersive (WD)-XRF reference element concentrations. For these, 38 bulk sediment samples were chosen to cover a range of lithologies based on the XRF scan, then 1 cm^3 dried ground sample was mixed with a lithium tetraborate/lithium metaborate flux and fused into 39-mm-diameter beads. Major element abundances were analysed by WD-XRF using a Bruker S8 Tiger spectrometer at Geoscience Australia. Loss on ignition was measured by gravimetry after combustion at 1,000 °C. One in every ten samples was duplicated along with multiple analyses of three international standards (NCS DC70306, MAG-1, ML-2) and an internal basalt standard (WG1). Quantification limits for all major element oxides are <0.2% and reproducibility is within 1%.

ARM. ODP Site 967 U-channel samples were sliced at 1-cm intervals into discrete non-magnetic 2 × 2 × 2 cm plastic cubes and measured for ARM on a 2G Enterprises cryogenic magnetometer at the Australian National University. The ARM was imparted using an alternating field of 100 mT and a direct current bias field of 0.05 mT.

Mediterranean evolution. Evaporative Mediterranean drawdown during the Messinian left residual brines in the adjacent eMed and wMed basins, with thicknesses reaching more than 2 km in the deepest parts[9,32,44]. We assume a water level drop of 2,000 m below Atlantic sea level in the eastern basin and 1,750 m in the western basin prior to the megaflood[5,8–10]. To relate Mediterranean refilling to the volume flux of the incoming flood, we use an intermediate reconstruction between Miocene and present-day Mediterranean hypsometry[10]. Before the flood, halite precipitation occurred at ~5.6 Ma in both basins at the MSC peak. The final MSC stage contains gypsum deposition punctuated by surface-water freshening events. A few drilling sites record gypsum below the flooding surface (Supplementary Table 1). Considering these observations, we set Messinian residual brine salinity to gypsum saturation at the start of the flood (140 PSU)[52]. We test model outputs for a range of starting salinities (60–240 PSU) in a sensitivity test (Extended Data Figs. 9 and 10).

The flooding phase. To determine the flood velocity entering the western basin from the Strait of Gibraltar, we use a flood incision model, following ref. [3]. This model computes the incision rate (dz_s/dt) at Camarinal sill based on the following approach, where dt is the timestep and dz_s is the depth of erosion per time step:

$$\frac{dz_s}{dt} = k_b(\tau_b)^a, \tag{1}$$

where k_b and a = 1.5 are positive constants. To obtain a final sill incision depth (240 m; ref. [3]), we calibrate k_b to $1.8 \times 10^{-4}\,m\,yr^{-1}\,Pa^{-a}$, where a is the constant mentioned above, while τ_b is the basal shear stress at the sill, which is computed using:

$$\tau_b = \rho_s g\,(z_s - z_0)\,S, \tag{2}$$

where ρ_s is seawater density, $(z_s - z_0)$ is the mean water depth at the sill, g is acceleration due to gravity and $S = z_h/L$ is the ratio between head loss (z_h) and length of the erosive channel (L). Manning's formula[3] is used to calculate the flow velocity:

$$v = \frac{1}{n} R_h^{\frac{2}{3}}\; S^{\frac{1}{2}}, \tag{3}$$

where v is the average flow velocity along the slope towards the Alboran basin, n = 0.05 is the roughness coefficient[3] and R_h is the hydraulic radius of the passage between the Atlantic and Mediterranean[3]. Where channel width is substantially greater than the water depth, the hydraulic radius is approximated by $(z_s - z_0)$. Flood discharge flux into the Mediterranean (Q) is then calculated using:

$$Q = W\,(z_s - z_0)\,v, \tag{4}$$

where $W = k_w Q^{a_w}$ is the incision channel width, which increases to a final 14 km value at the end of the flood. Here a_w = 0.5 is a constant, and we impose k_w = 1.1 to obtain the final channel width (see Methods in ref. [3] for details).

This model predicts a peak discharge flux that exceeds 100 Sv at a velocity >40 m s^{-1} at the Camarinal sill[3]. In the initial flood stage, high-energy normal Atlantic seawater inflow encounters much denser residual wMed brines. The extent of mixing between brine and floodwaters depends on the kinetic energy of the flow that approaches the brine surface. Without mixing, a seawater layer (ρ_s) would form on top of the denser brine (ρ_b). In contrast, if complete seawater mixing occurred with the brine, a single intermediate density layer (ρ_m) would have formed. Mixing due to turbulent erosion of stratification can be accomplished with a large enough energy to overcome the potential energy, raising denser fluid parcels while lowering lighter parcels[53].

If complete mixing occurred in the basin, the centre of gravity of the system must be raised, resulting in a potential energy gain given by:

$$\begin{aligned} PE_{Final} - PE_{Initial} = PE_{Gain} = \int_0^{H+h} \rho_m g z dz A\,(z) \\ - \left(\int_H^{H+h} \rho_s g z dz A\,(z) + \int_0^H \rho_b g z dz A\,(z) \right), \end{aligned} \tag{5}$$

where PE_{Gain} represents the energy (per day) required for complete mixing, $A(z)$ is the basin surface area with depth (z), h is the thickness of the seawater layer flooded into the basin per timestep (per day) and H is the total brine column thickness prior to mixing.

Under the assumption of the model in ref. [3] that the slope of Atlantic water inflow into the wMed is constant over time, the flow velocity entering the brine surface in the western basin, v_{wMed} is v. The kinetic energy per day of this inflow (KE_{wMed}) is then calculated using:

$$KE_{wMed} = \frac{1}{2}\rho_s v_{wMed}^2 Q. \tag{6}$$

In our model, we calculate energy conversions at daily iterations, by integrating the energy expression in equation (6) over one-day intervals. Available potential energy of inflow into the wMed (at the sill), APE_{wMed}, is equal to $\rho_s g Q L_{wMed}$, where L_{wMed} is the vertical distance between the brine surface and the Camarinal sill crest. As the Atlantic inflow descended downslope, gravitational potential energy was released to kinetic energy and was lost in processes such as Zanclean channel erosion and turbulent dissipation. Erosion along the slope will have resulted in a headward-migrating erosion wave along the channel that may have then triggered even higher flow and erosion rates, resulting in a more abrupt flood[54]. Therefore, our calculations offer a minimum estimate of flow kinetic energy into the wMed.

Most of the inflow kinetic energy into the basin is lost to viscous turbulent dissipation. Laboratory experiments in stratified fluids suggest that ~20% of the turbulent energy loss goes to irreversibly mixing the stratification (known as the mixing efficiency)[55,56]. Thus, the energy available for basin mixing (KE_{Av}) can be given as:

$$KE_{Av} = \Gamma \times KE_{wMed}, \tag{7}$$

where $\Gamma \approx 0.2$ is the mixing efficiency. Full-depth mixing can occur only if $KE_{Av} > PE_{Gain}$. If available kinetic energy is less than that required to mix the entire brine column thickness (H), partial brine mixing will occur. The mixing extent can then be computed using energy arguments. For this purpose, we introduce a mixing depth (H_{Mix}). Where mixing is incomplete, equation (7) can be rewritten as:

$$\begin{aligned} KE_{Av} = PE_{GPar} = \int_{H+h-H_{Mix}}^{H+h} \rho_m g z dz A(z) \\ - \left(\int_H^{H+h} \rho_s g z dz A\,(z) + \int_{H+h-H_{Mix}}^{H} \rho_b g z dz A\,(z) \right), \end{aligned} \tag{8}$$

where PE_{GPar} is the potential energy gain during partial mixing. Hence, if available energy is insufficient to mix completely, mixing will be restricted to a brine depth of H_{Mix}. If the flow kinetic energy increases with time, H_{Mix} will increase accordingly, eventually completely mixing the brine when KE_{Av} exceeds PE_{Gain}.

We use the following approach to calculate the salinity evolution (S_m) of the mixed fluid:

$$S_m = \frac{QS_{AW} + Q_b S_b}{Q_m} = S_{wMed}, \tag{9}$$

where Q_b is the brine volume (per day) mixed in the basin, S_{AW} *is the Atlantic water salinity*, S_b is the brine salinity and Q_m is the resultant volume of mixed fluid (per day). For salinity–density conversions, we include the Gibbs Sea Water (GSW) Oceanographic Toolbox functions into our model.

Once wMed sea level reaches the Sicily sill (430 m below sea level), wMed mixed fluid spills into the eMed. We use equation (8) to compute the mixing extent in the eastern basin as it fills. Noto Canyon is considered to be the path of flood waters into the Ionian basin (eMed) during the megaflood[15]. To approximate the flow velocity approaching the eMed brine surface, we consider that the volume flux spreads across a channel of width b_{eMed}, in a fluid layer of depth d_{eMed} travelling at velocity v_{eMed}. The erosive channel detected at the upper Noto Canyon is 4 km wide; thus, we impose b_{eMed} to be a 4 km maximum. The present average channel depth is 400 m (refs. [15,16]) (d_{eMed}). Minimum flow velocity into the eMed is then given by:

$$v_{eMed} = \frac{Q}{A_{Noto}}, \tag{10}$$

where A_{Noto} is the present-day maximum cross-sectional area of the Noto Canyon erosive channel. In reality, flow velocity entering the eMed would have been higher due to the steep slope towards the end of the passage[15,16]. The kinetic energy of flow entering the brine is:

$$\mathrm{KE_{eMed}} = \frac{1}{2}\rho_s\left(v_{\mathrm{eMed}}^2\right)Q. \tag{11}$$

Similar to the wMed approach, complete mixing is assumed if $1 > (\Gamma\,\mathrm{KE_{eMed}})/\mathrm{PE_{Gain}}$. As the eMed is filled, wMed waters mix continuously due to inflow through the Strait of Gibraltar. Equation (9) is used to calculate salinity evolution in both basins during this flood stage (S_{wMed} and S_{eMed}, respectively). The water flow cascading into the Ionian basin (eMed) terminates once the eMed level reaches the Sicily sill level. Thereafter, both eMed and wMed levels rise simultaneously to the Atlantic level. In this final flood stage, mixing occurs due to flow along the Zanclean channel (Strait of Gibraltar), further diluting the western basin (thus, further decreasing S_{wMed}).

The evolving phase. During the first part of our model (flooding phase), most wMed salt was transferred into the eMed across the Strait of Sicily. As a result, the wMed had less saline waters, whereas the eMed filled with a denser brine layer up to the Sicily sill (the reconstructed early Pliocene eMed volume with sea level equal to the Sicily sill level is 2.04×10^{15} m^3; ref. [10]). For the Mediterranean to return to normal marine conditions, this enormous amount of brine should then have been redirected to the Atlantic Ocean.

The processes required to erode this deep, dense brine layer would have involved mixing across the interface separating it from inflowing waters. This mixing would occur due to the same set of processes that operate in the modern global ocean; namely, diapycnal mixing due to internal wave breaking[47,57]. Generation of internal gravity waves results from a chain of processes including barotropic tidal flow over topography, variations in wind force at the ocean surface, lee waves produced by ocean currents and eddies flowing over topography[47,57]. The sum of all turbulent processes leads to an effective turbulent diffusivity of $K_S = 1{-}5\times10^{-5}$ m^2 s^{-1} (refs. [48,57]). By assuming a turbulent diffusivity in this range, we estimate the duration required to erode the deep layer. The salinity profile immediately after the flooding event consists of an upper Mediterranean seawater layer and a deep brine layer below the sill depth. Mixing and advection is rapid in the x and y directions (horizontally); thus, a good approximation for salinity, S, at any time is that it depends on height, z, only. The diffusive timescale, t, can be estimated from the diffusion equation:

$$\frac{\partial S}{\partial t} = K_S\frac{\partial^2 S}{\partial z^2}. \tag{12}$$

To solve equation (12) numerically, we divide the domain into N equally spaced layers, each having thickness d_z. Basin hypsometry is characterized by the surface area (A_z) at each depth interval. The salt flux between adjacent layers is proportional to the local salinity gradient given by:

$$F \approx K_S\frac{\partial S}{\partial z}. \tag{13}$$

Evolution of salinity in the jth layer of the domain is given by the flux divergence:

$$A^j\frac{\partial S^j}{\partial t} = \frac{K_S}{d_z}\left(A^{j+1}\left[\frac{S^{j+1}-S^j}{d_z}\right] - A^j\left[\frac{S^j-S^{j-1}}{d_z}\right]\right). \tag{14}$$

When this equation is further discretized in time, it can be shown that:

$$S^j_{\tau+1} = S^j_{\tau-1} + \frac{2K_S d_t}{d_z^2}\left(S^{j-1}_\tau - \left[\frac{A^{j+1}}{A^j}+1\right]S^j_\tau + \left[\frac{A^{j+1}}{A^j}\right]S^{j+1}_\tau\right), \tag{15}$$

where d_t is the time step and time levels are indicated by the subscript (τ). With use of these equations, we compute the salinity profile evolution until the basin reached modern eMed salinity values. Diffusive transport of salt from deeper layers to upper eastern basin layers will be balanced by salt transport to the wMed and ultimately into the Atlantic Ocean via the Mediterranean outflow.

Sensitivity test part 1: basin evolution for a largely refilled Mediterranean (alternative hypothesis). The nature of the MSC termination has long been debated. One hypothesis is a catastrophic termination (the main scenario of this paper) that resulted from Camarinal sill collapse in the Strait of Gibraltar[3,11,15,16]. This hypothesis considers a kilometre-scale drawdown of water in Mediterranean sub-basins prior to the reconnection. An alternative hypothesis interprets an almost-filled Mediterranean during the final MSC stage (Lago Mare), which was connected to the Atlantic and/or Paratethys prior to the termination[12,14,58].

Here we present a sensitivity test to evaluate the validity of our hypothesis (a partially desiccated Mediterranean leading to catastrophic termination), compared with a scenario where the basin is filled to the Sicily sill before the termination. We argue that the sapropel presence immediately after the M/P boundary in eMed cores (Supplementary Table 1) resulted from basin stratification after the Zanclean megaflood. In contrast, no wMed sapropels were found following the M/P boundary. We suggest that absence of a wMed sapropel resulted from brine transfer to the eMed during an abrupt refilling event.

If the present-day Black and Caspian seas were completely emptied into the Mediterranean, this would result in a ~250-m-thick layer at the Mediterranean surface[13]. This gives a high-end estimate of Paratethyan inflow to the Mediterranean if the two basins were connected during the Lago Mare phase. It has been suggested that gypsum precipitation resulted from evaporated Paratethyan surface waters (above denser residual brines) at a salinity of ~40 PSU[58]. Therefore, we simulate emptying of a volume equivalent to the present-day Black and Caspian seas into the Mediterranean and allow it to evaporate to a salinity of 40 PSU. If the top of such a layer sits at the crest of the Sicily sill (430 m), it will be about 130 m in thickness (calculated using a reconstructed Mediterranean hypsometry[10]) and will extend below the sill crest to a depth of 560 m.

Numerical modelling has shown that halite precipitation during the MSC peak (Stage 2, 5.59–5.55 Ma) resulted from complete disconnection from the Atlantic[59]. Complete isolation will result in basin drawdown due to excess evaporation that will come to equilibrium within a few thousand years (3,000–8,000 years)[9,10]. The idea of a kilometre-scale drawdown is also supported by the existence of a basin-wide Messinian erosional surface[5] and deep canyons excavated beneath the Nile delta and Rhône River mouth[6,7]. Similar to our main scenario, we assume a wMed deep brine layer at gypsum saturation (140 PSU) below 1,750 m, which formed as a result of MSC Stage 2 drawdown. From 560 m to 1,750 m, we allow salinity to increase linearly from 40 to 140 PSU, to obtain a conservative estimate (Extended Data Fig. 6a).

Starting with this basin configuration, we compute wMed basin evolution (Extended Data Fig. 6b) during a refilling event resulting from inflow through the Strait of Gibraltar using the flooding phase model. Here we re-calibrate the channel width coefficient (k_w) to allow the inflow channel to evolve up to the same dimensions as in our main scenario. We then compare the refilling and basin evolution in both scenarios (Extended Data Fig. 6c). Our findings suggest that for a filled Mediterranean up to the crest of the Sicily sill, reconnection with the Atlantic results in a much longer episode of refilling. The total kinetic energy released during such a scenario will be >50 times smaller compared with a catastrophic termination, which is insufficient to erode the deeper brine in the wMed and would result in persistence of a density-stratified wMed (Extended Data Fig. 6b,c). In that case, we argue that a sapropel should be expected in the wMed after Atlantic reconnection. Absence of a wMed sapropel provides strong support for catastrophic MSC termination and for a drawn-down Mediterranean prior to Atlantic reconnection. We also test this scenario for even lower salinity profiles between a thin surface layer and deep brines (from 560 m to 1,750 m), to assess if the flood energy was sufficient to erode wMed deep brines, if the mid-layer salinity was lower (Extended Data Fig. 7a,b). This test run confirms that the energy is insufficient to remove wMed deep brines even for a 100% mixing efficiency.

Sensitivity test part 2: basin evolution at initial salinities <140 PSU (main scenario). To test the validity of our hypothesis in case the residual Messinian fluid salinity was lower than 140 PSU, we computed the salinity evolution of the wMed and eMed using the same approach in the flooding phase used for the main scenario. We use a range of salinities from 60 to 120 PSU. Then we use the evolving phase to determine the duration of brine removal at different initial salinities (Extended Data Fig. 7c,d). At salinities lower than 140 PSU, all wMed salt is transferred to the eMed, resulting in a salinity approximated by:

$$S_{\mathrm{eMed}} = \frac{\left(V_{\mathrm{eMed(Sicily)}} - V_{\mathrm{b(eMed)}} - V_{\mathrm{b(wMed)}}\right)\times S_{\mathrm{AW}} + \left(V_{\mathrm{b(eMed)}} + V_{\mathrm{b(wMed)}}\right)\times S_{\mathrm{b}}}{V_{\mathrm{eMed(Sicily)}}} \tag{16}$$

where S_{eMed} is the final eMed salinity below the Sicily sill, $V_{eMed(Sicily)}$ is the total eMed volume at the Sicily sill, $V_{b(eMed)}$ and $V_{b(wMed)}$ are the residual Messinian volumes in eMed and wMed, respectively, and S_b is the initial Mediterranean fluid salinity. For a range of initial residual Messinian brine salinities from 60 to 120 PSU, we find that the salt removal period varies between ~14,000 to 22,000 years.

Sensitivity test part 3: basin evolution at initial salinities >140 PSU (main scenario). To test the validity of the hypothesis in case the residual Messinian salinities were >140 PSU, we compute the salinity evolution of the wMed and eMed using flooding phase calculations for 160–240 PSU. We employ the evolving mode approach to estimate salt removal duration for both basins, when excess salt remains at the end of the flooding phase. If wMed stratification was less than the resulting winter water density, convective overturn would mix surface and deep waters, removing the additional salt. In the present-day wMed, surface salinities reach 38.0–38.4 PSU in winter, with reduced temperatures of 10–12 °C (ref. [29]). We assume a constant brine temperature of 20 °C during the flooding phase. Therefore, we calculate the sea water salinity at 20 °C for an equivalent wMed winter surface-water density. We use this as a limit in determining the brine removal period in the evolving phase (Extended Data Fig. 8). Results of the sensitivity test indicate that all wMed salt would transfer to the eMed up to initial brine salinities of 170 PSU. From 170 to 200 PSU, final mixed wMed waters have a higher-than-winter water density. Above 220 PSU, residual Messinian brines remain in the deep wMed, implying that flood energy was insufficient to erode the deep brines. Above 170 PSU initial salinity, we find that it would take about 4,000 to 12,000 years to remove wMed salt by diffusion. Combining the information from sensitivity test parts 2 and 3, we conclude that our model results agree reasonably with the data for starting salinities across the 60–170 PSU range.

Sensitivity test part 4: basin evolution with the change of Sicily sill depth. To test the effect of Sicily sill depth on basin evolution during the flooding mode, we modified our model for shallower and deeper than present Sicily sill depth. For this, we employed ~0.7 and ~1.3 times the present sill depth (300 m and 560 m, respectively). We find that the flooding mode length reduces/increases when the Sicily sill depth is shallower/deeper than present. We find that independent of the sill depth, a majority of the wMed Messinian salt is transferred to the eMed across the sill (Extended Data Fig. 9). Our model suggests that as the sill gets shallower, there is slightly more salt remaining in the wMed, compared with the deeper sill setting. Detailed palaeomagnetic studies have shown that the Sicily sill may have been uplifted to its present depth during central to eMed-wide middle–late Pliocene tectonic events[24,60]. Modelling experiments have also suggested a deeper Sicily sill during the Messinian[9,10,14]. Our model results would agree with these observations, as more wMed salt would be transferred to the eMed for a deeper sill.

Sensitivity test part 5: effect of the initial base level on basin evolution. We have assumed initial base levels for the wMed (1,750 m below Atlantic level) and the eMed (2,000 m) for our main scenario, based on available references. In sensitivity test part 1 (alternative scenario), we tested basin evolution when the Mediterranean is filled up to the Sicily sill. To test the effect of intermediate base levels, and to define a minimum base level that validates the hypothesis, we computed basin evolution by stepwise increasing the base level in 100 m increments in both basins. For each step of base level increase above the main scenario base levels, we filled both wMed and eMed with lower-salinity waters following the steps of sensitivity test part 1. From 1,750 m up to 1,450 m base level in the wMed (2,000 to 1,700 m in the eMed), all the residual Messinian salt is transferred from wMed to the eMed. When the base level is increased above this point, excess salt tends to remain in the wMed. We have shown test results up to 1,250 m wMed base level, corresponding to a 1,500 m eMed base level (Extended Data Fig. 10). A period of 2,500 to 4,500 years is required to remove the excess salt by diffusion when the wMed level is above 1,450 m.

Data availability

ODP Site 967 data from this study are available from Panagea (www.pangaea.de) under 'Scanning XRF and environmental magnetic data across the Miocene-Pliocene boundary from ODP Site 967 (eastern Mediterranean)' and are also available as online Supplementary Data accompanying this article. Source data are provided with this paper.

Code availability

All the figures in this manuscript are reproducible via Jupyter notebooks and instructions provided in the Github repository Med_evolution_megaflood[61] (https://doi.org/10.5281/zenodo.6528768).

References

51. Weltje, G. J. et al. in *Micro-XRF Studies of Sediment Cores* (eds. Croudace, I. W. & Rothwell, R. G.) 507–534 (Springer, 2015).
52. Rohling, E. J., Schiebel, R. & Siddall, M. Controls on Messinian lower evaporite cycles in the Mediterranean. *Earth Planet. Sci. Lett.* **275**, 165–171 (2008).
53. Cushman-Roisin, B. & Beckers, J.-M. *Introduction to Geophysical Fluid Dynamics: Physical and Numerical Aspects* (Academic Press, 2011).
54. Garcia-Castellanos, D. & O'Connor, J. E. Outburst floods provide erodability estimates consistent with long-term landscape evolution. *Sci. Rep.* **8**, 10573 (2018).
55. Peltier, W. R. & Caulfield, C. P. Mixing efficiency in stratified shear flows. *Annu. Rev. Fluid Mech.* **35**, 135–167 (2003).
56. Osborne, T. Estimates of the local rate of vertical diffusion from dissipation measurements. *J. Phys. Oceanogr.* **10**, 83–89 (1980).
57. MacKinnon, J. A. et al. Climate process team on internal wave-driven ocean mixing. *Bull. Am. Meteorol. Soc.* **98**, 2429–2454 (2017).
58. Grothe, A. et al. Paratethys pacing of the Messinian salinity crisis: low salinity waters contributing to gypsum precipitation? *Earth Planet. Sci. Lett.* **532**, 116029 (2020).
59. Garcia-Castellanos, D. & Villaseñor, A. Messinian salinity crisis regulated by competing tectonics and erosion at the Gibraltar arc. *Nature* **480**, 359–363 (2011).
60. Duermeijer, C. E. & Langereis, C. G. Astronomical dating of a tectonic rotation on Sicily and consequences for the timing and extent of a middle Pliocene deformation phase. *Tectonophysics* **298**, 243–258 (1998).
61. Amarathunga, U. & Hogg, A. M. Resurgence of Mediterranean after the Zanclean megaflood - Jupyter notebooks (Python). *Zenodo* https://doi.org/10.5281/zenodo.6528768 (2022).
62. Grant, K. M. et al. A 3 million year index for North African humidity/aridity and the implication of potential pan-African humid periods. *Quat. Sci. Rev.* **171**, 100–118 (2017).
63. Laskar, J., Fienga, A., Gastineau, M. & Manche, H. La2010: a new orbital solution for the long-term motion of the Earth. *Astron. Astrophys.* **532**, A89 (2011).

Acknowledgements

We thank D. Garcia-Castellanos for providing essential instructions on developing the Mediterranean reflooding model. We also thank P. Meijer for providing the latest Mediterranean hypsometry reconstruction. Study material on fluid dynamics provided by B. Cushman-Roisin encouraged initial model development. This work contributes to Australian Research Council projects FL120100050 and DP2000101157 (E.J.R.), DE190100042 (K.M.G.), DP190100874 (A.P.R.), and the Australia-New Zealand IODP Consortium (ANZIC) Legacy/Special Analytical Funding grant LE160100067 (Katharine Mary Grant (K.M.G.), Laura Rodriguez Sanz (L.R.S.)).

Author contributions

U.A. designed and led the study and wrote the paper; U.A. developed the hypothesis and performed the modelling, with guidance from A.M.H. and E.J.R.; E.J.R., A.M.H., A.P.R., K.M.G. and D.H. contributed to data interpretation; K.M.G. calibrated scanning XRF data; S.G. performed WD-XRF analyses; X.Z. and P.H. assisted with magnetic measurements; D.L. performed XRF core scanning; D.L. and T.W. developed the ODP967 composite depth splice; all authors contributed to manuscript development.

Competing interests

The authors declare no competing interests.

Additional information

Extended data is available for this paper at https://doi.org/10.1038/s41561-022-00998-z.

Supplementary information The online version contains supplementary material available at https://doi.org/10.1038/s41561-022-00998-z.

Correspondence and requests for materials should be addressed to Udara Amarathunga.

Peer review information *Nature Geoscience* thanks Angelo Camerlenghi, Rachel Flecker and the other, anonymous, reviewer(s) for their contribution to the peer review of this work. Primary Handling Editor: James Super, in collaboration with the *Nature Geoscience* team.

Reprints and permissions information is available at www.nature.com/reprints.

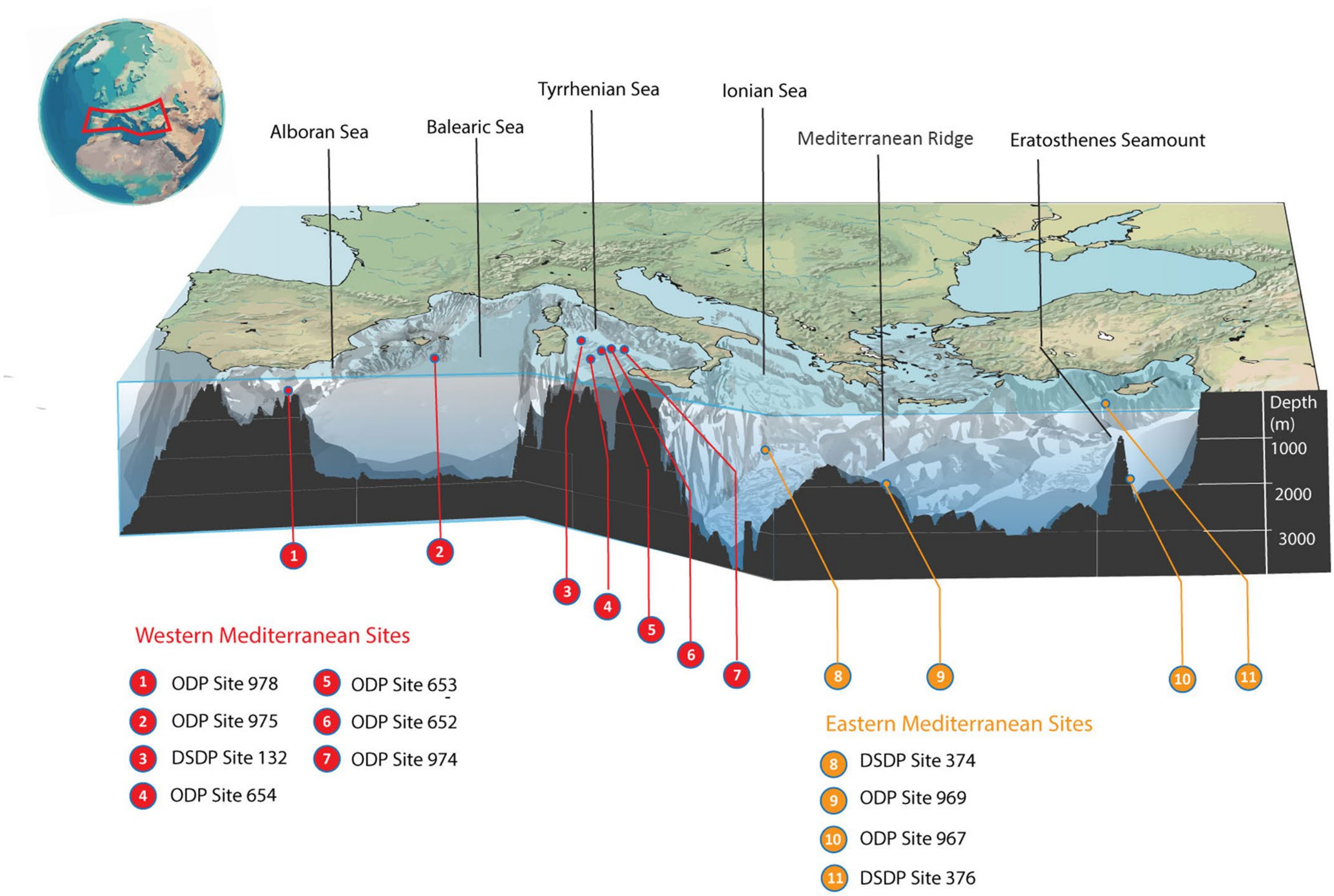

Extended Data Fig. 1 | Locations of DSDP and ODP sites with complete records across the Miocene-Pliocene transition. Illustration of the Mediterranean basin with locations of ODP and DSDP sites where complete records across the Miocene/Pliocene boundary have been retrieved (see Supplementary Table 1). XRF core scanning data for this study were obtained from ODP Site 967 (Eratosthenes Seamount northern flanks). The cross-section was drawn using Ocean Data View 5.3.0.

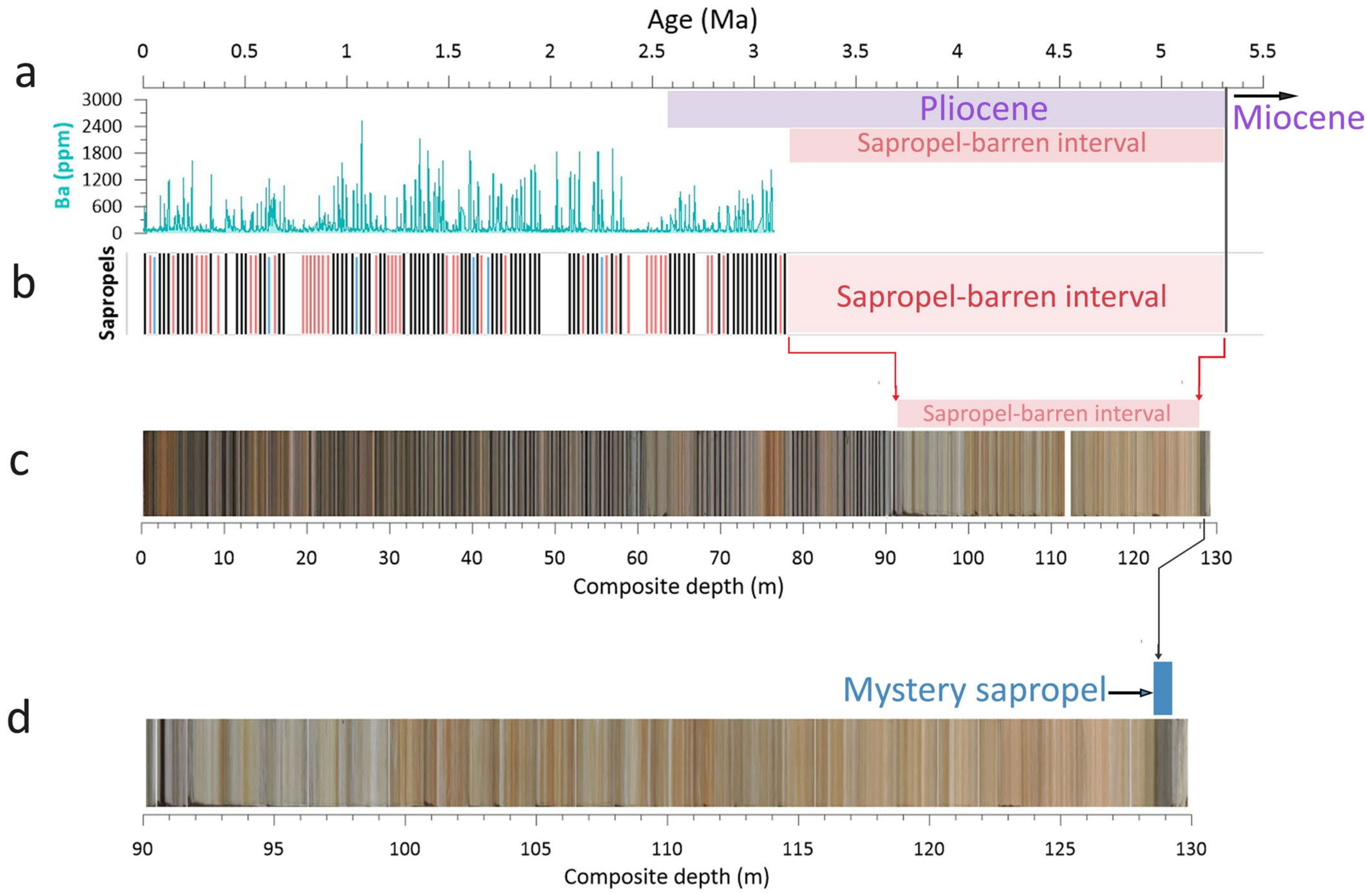

Extended Data Fig. 2 | Sapropel record for ODP Site 967. a, Ba record for ODP967 from scanning XRF data for the last 3 million years[62]. **b**, Sapropel stratigraphy for ODP Site 967. From 5.3 to 3.2 Ma[23], sediments are barren of sapropels (black = sapropels, red = red intervals, blue = ghost sapropels). **c**, Stack of core images for ODP967 arranged according to composite depth, with sapropel occurrence. Sapropel-barren interval is indicated by the section shaded in pink. d, Enlarged view of the sapropel-barren interval. Location of the 'mystery sapropel' is indicated by blue shading.

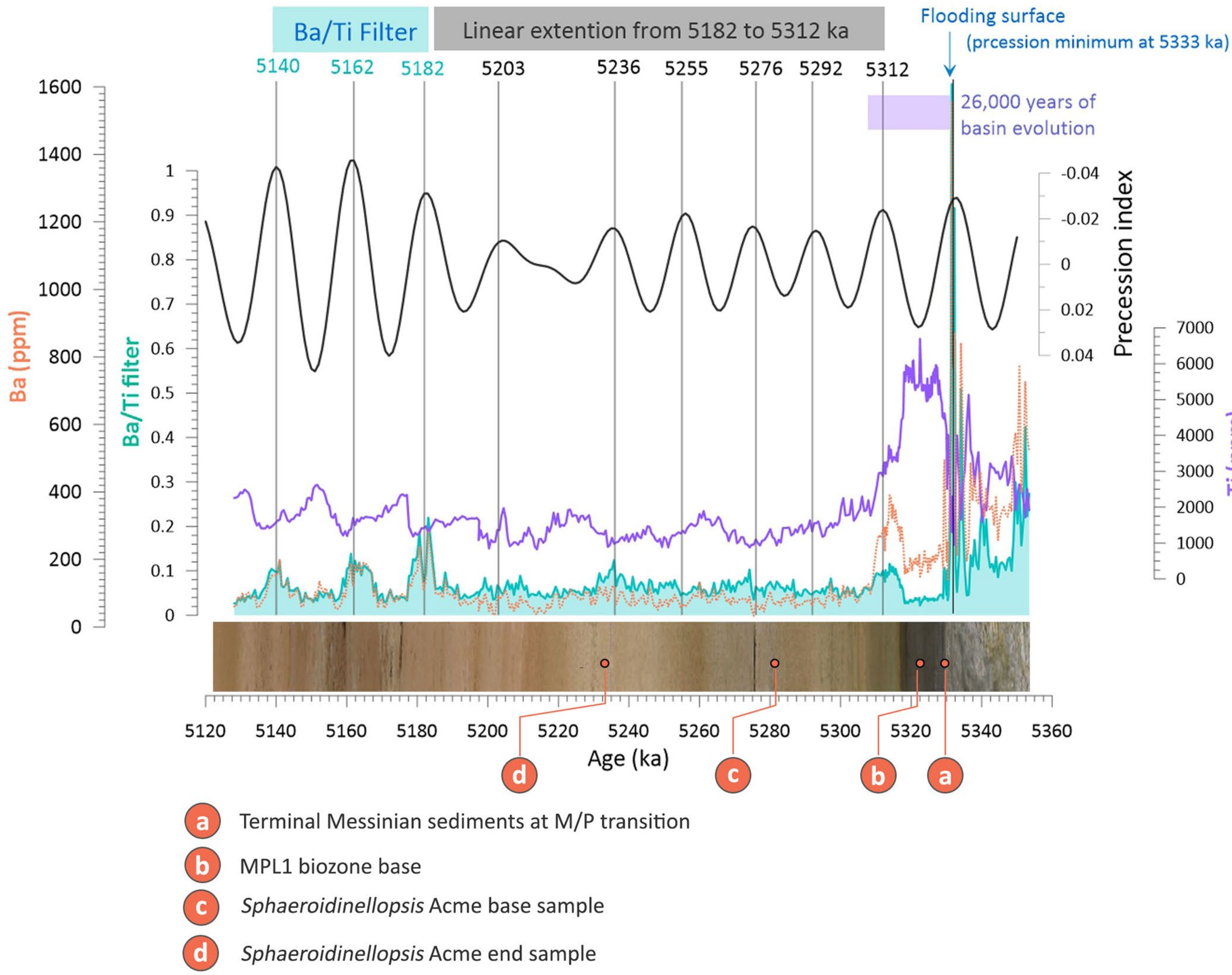

Extended Data Fig. 3 | Chronology. Three peaks in the Ba/Ti record were tuned to insolation maxima (precession minima, June 21, 65°N)[63] between 5140 and 5182 ka. Below this (splice depth 125.03–127.23 m), clear Ba/Ti peaks are absent, so ages were interpolated linearly assuming a sedimentation rate equivalent to that for 5162–5182 ka. This assumption is validated by the resulting insolation maximum alignment at 5312 ka (splice depth 127.23 m) with the next Ba/Ti peak. The succeeding Ba peak (at splice depth 128.35 m) is the largest, so the maximum of the smoothed curve was tuned to 5333 ka based on the timing of the Mediterranean reflooding event[3]. Available ODP 967 biostratigraphic datums[22] (a, b, c, d) validate our chronology (see Supplementary Table 2 for details).

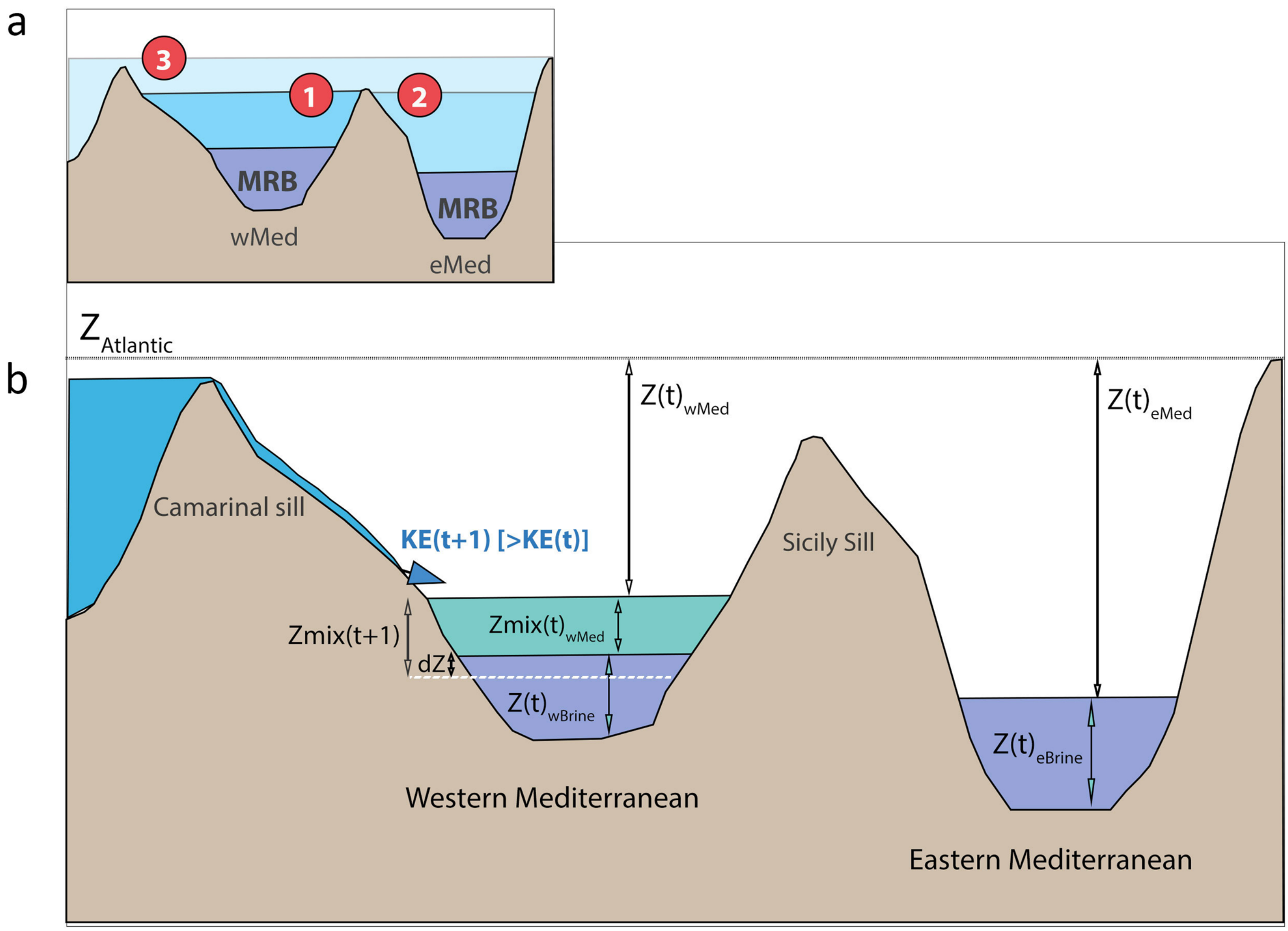

Extended Data Fig. 4 | Conceptual model for Mediterranean refilling. a, Sketch of main Zanclean flooding stages (ZFS). ZFS 1 ends as the wMed level reaches the Sicily Sill. ZFS 2 ends as the eMed level reaches Sicily Sill. In ZFS 3, both basins rise to the Atlantic level concurrently. MRB, Messinian Residual Brines; wMed, Western Mediterranean; eMed, Eastern Mediterranean. **b**, Sketch of basin evolution during the flooding phase. As flood waters flow into the basin, mixing with residual brines (purple) occurs. The mixing extent depends on the kinetic energy of flow entering the brine surface. For increased kinetic energy, a *dz* depth of brines will be added to the mixed layer (green). The mixed layer thickness increases accordingly. KE(t + 1), kinetic energy of flow entering the brine; KE(t), kinetic energy of flow in the previous timestep; $Z(t)_{wMed}$, wMed level at a given time; $Z(t)_{eMed}$, eMed level at a given time; $Zmix(t)_{wMed}$, wMed mixed layer extent at a given time; $Z(t)_{wBrine}$, wMed brine thickness at a given time; $Z(t)_{eBrine}$, eMed brine thickness at a given time; and $Z_{Atlantic}$, Atlantic level.

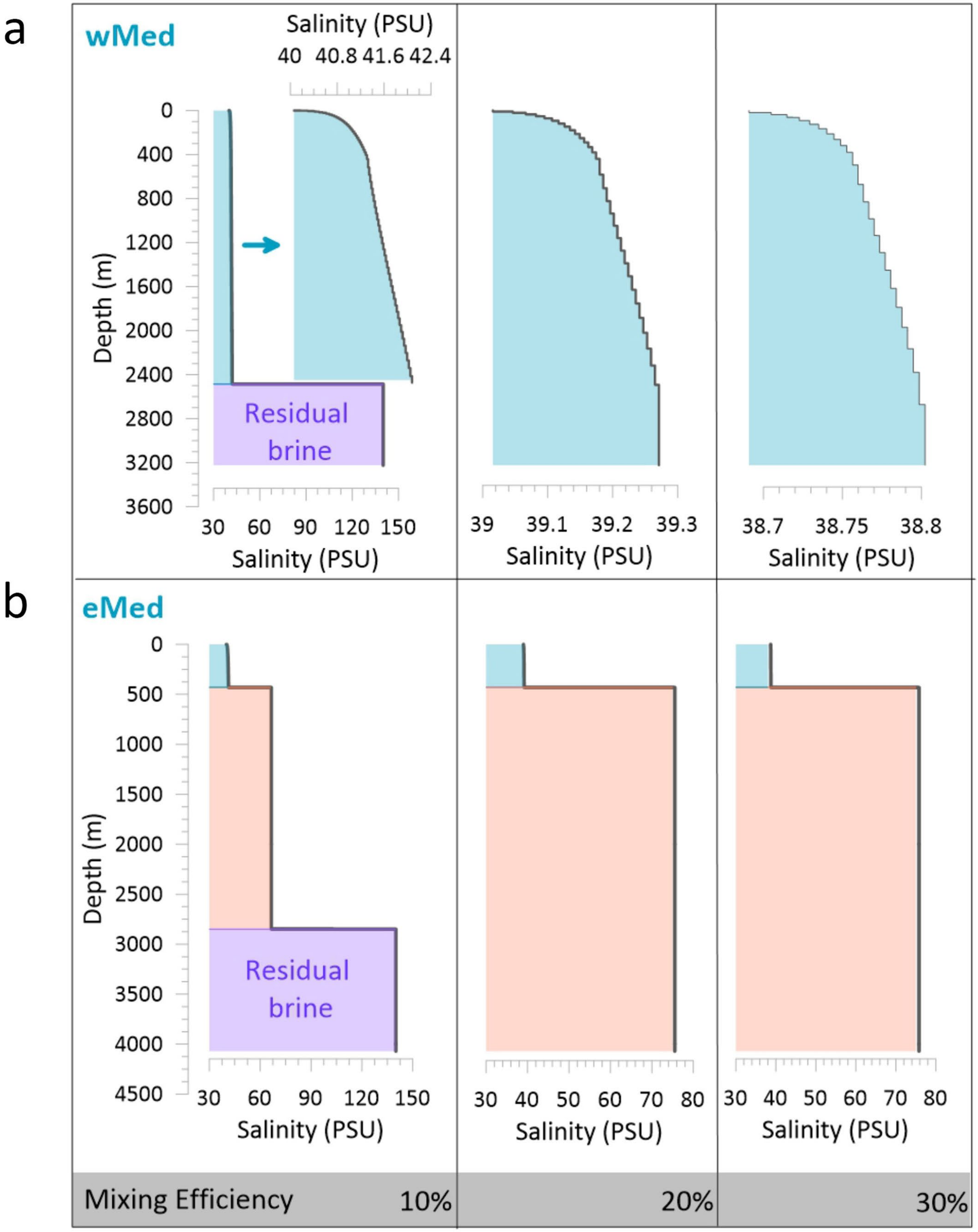

Extended Data Fig. 5 | See next page for caption.

Extended Data Fig. 5 | Salinity profiles for wMed and eMed at the end of the Flooding Phase for different ME values. For our main model, we use ME = 20% (0.2), which is the widely accepted value for shear-driven mixing in stratified fluids[55,56]. Here we test the effect of ME change on basin evolution, for the 10–30 % ME range. **a**, Salinity profiles (wMed) at the end of the Flooding Phase for different ME values. At 10% ME, a ~700-m-thick residual brine layer remains in the bottom of the wMed. The salinity profile above the pycnocline is enlarged in this case. For 20% and 30% ME, the wMed does not contain residual brine. **b**, Salinity profiles (eMed) at the end of the Flooding Phase for different ME values. For each ME value, strong stratification occurs at the Sicily Sill level, where dense fluids lie toward the bottom (salinity profile colours: blue-green = wMed mixed layer; orange = eMed mixed layer; purple = residual Messinian brines; during the final flood stage, mixing occurs only in the wMed, from which mixed waters overflow toward the eMed above Sicily Sill – indicated by an upper blue-green eMed layer).

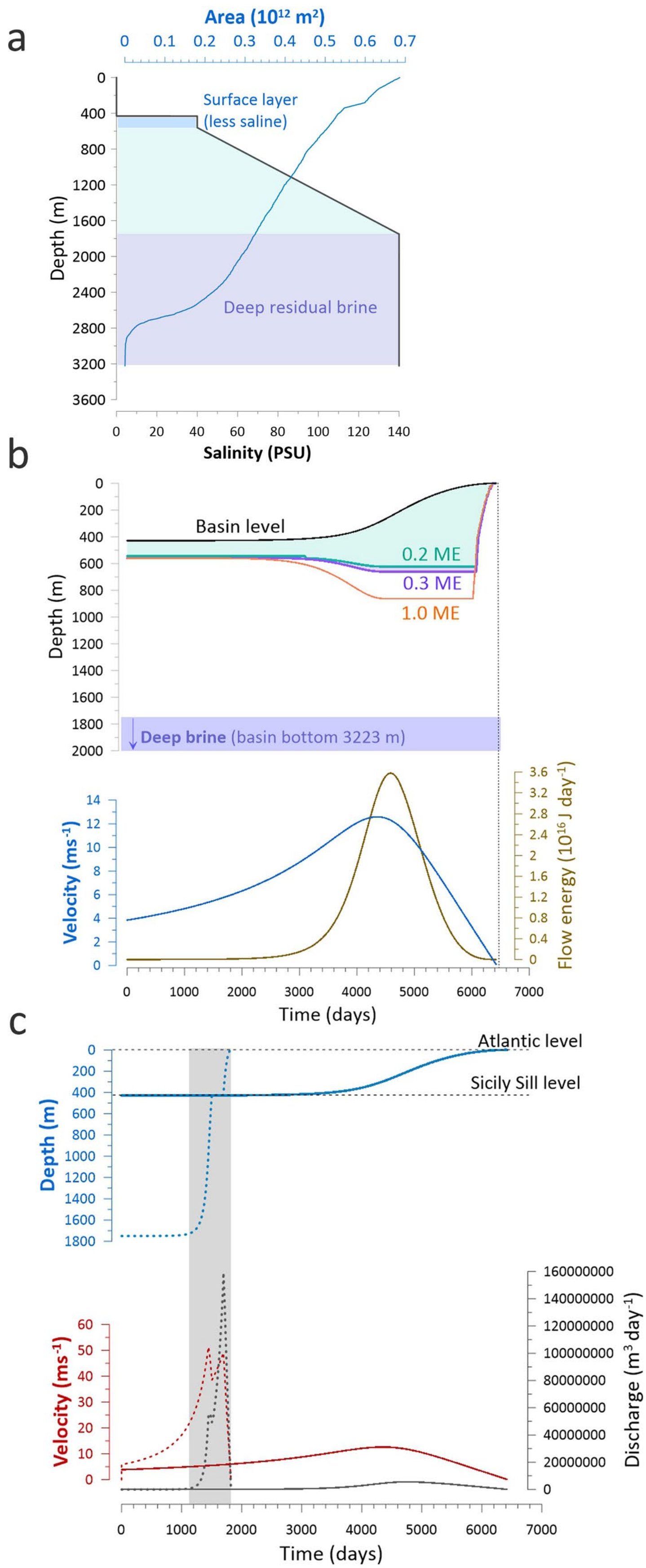

Extended Data Fig. 6 | See next page for caption.

Extended Data Fig. 6 | Summary of sensitivity test (Part 1) results. a, wMed salinity profile (black) where the basin is filled to the Sicily Sill level. The thin surface layer is composed of evaporated Paratethyan waters. Blue line is wMed hypsometry. **b**, Evolution of the wMed level (black), mixing depth at different mixing efficiencies (0.2, 0.3 and 1 ME), velocity and flow kinetic energy with time, for the basin configuration in a. Even at 100% mixing efficiency (1 ME), flow energy fails to erode the deep brine layer. **c**, Comparison of refilling abruptness between a scenario where the basin is filled to the Sicily Sill level (thick lines), and a deeply desiccated basin before the catastrophic termination (dotted lines). The length of the flooding mode increases to 6400 days for a filled basin, while discharge and flow velocity are much less compared to a catastrophic termination. The shaded section demarcates the interval (dotted lines) used to compute basin evolution in the main text.

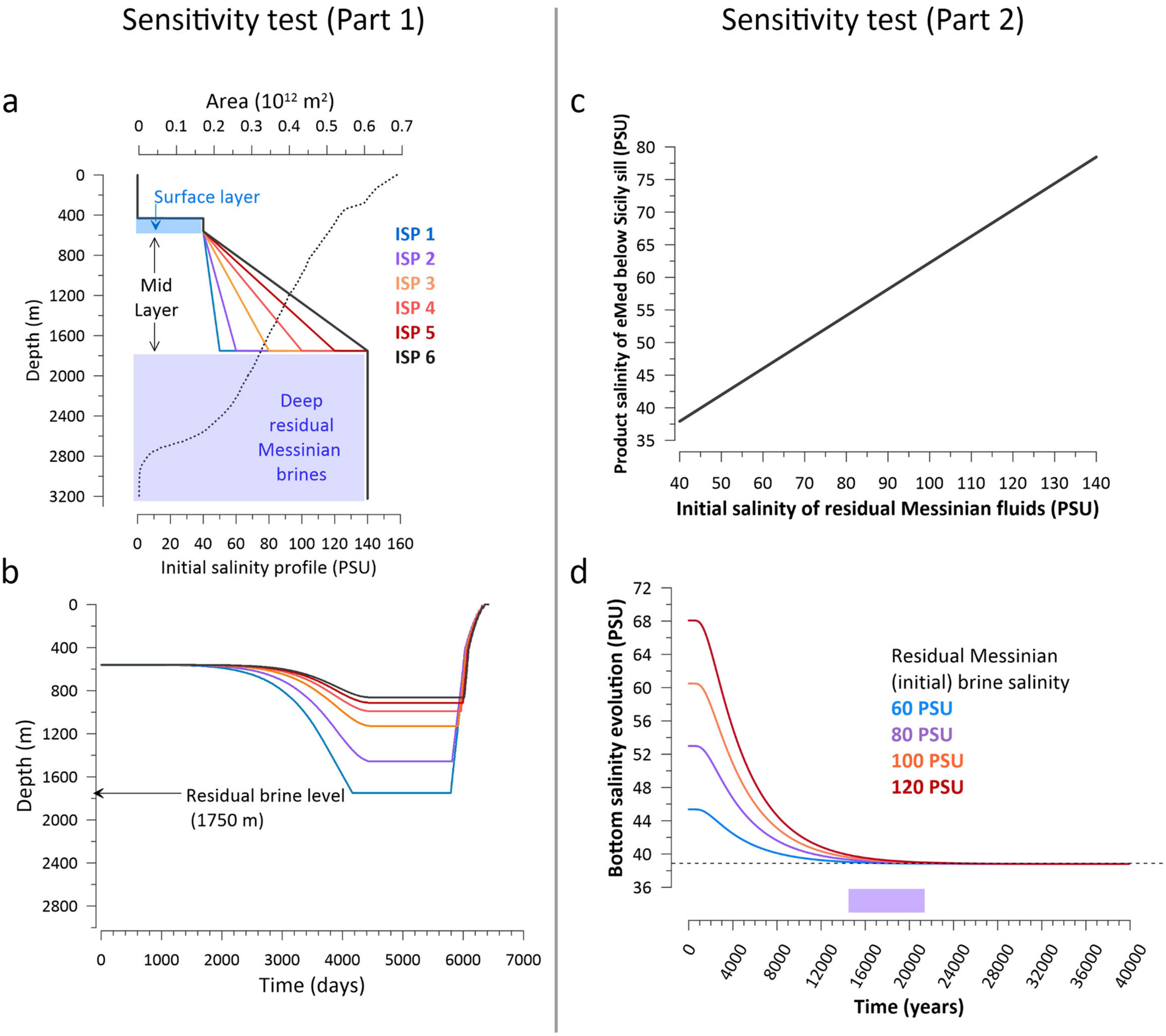

Extended Data Fig. 7 | Sensitivity test Part 1 and Part 2 results. (**a,b**; Sensitivity test Part 1 - Testing for different initial salinity profiles) **a**, Initial wMed salinity profiles used for the test; surface layer (430–560 m) and residual brine layer (below 1750 m) salinities were kept unchanged at 40 and 140 PSU, respectively. Mid-layer salinity was changed, as shown in the Figure (ISP 1 to ISP 6, ISP; initial salinity profile). For the mid-layer, salinity was increased linearly from 40 PSU at 560 m, to 50 PSU (ISP 1), 60 PSU (ISP 2), 80 PSU (ISP 3), 100 PSU (ISP 4), and 120 PSU (ISP 5), at the deep brine surface (1750 m). ISP 6 is the same as used in Extended Data Fig. 6. The black dotted line is wMed hypsometry. **b**, Evolution of the mixing depth at 100% mixing efficiency for different starting salinity profiles in a. For ISP 1, mixing depth reaches the brine surface, but the flood energy is insufficient to erode the brine layer. Maximum mixing depth does not extend below 1500 m for any other starting salinity profile, implying that the flood energy is insufficient to reach deep wMed brines below 1750 m. The same colours for ISPs are used for mixing depth evolution lines. The black dotted line indicates the wMed level rise as Atlantic waters fill the Mediterranean. (**c,d**; Sensitivity test Part 2) **c**, Approximation of the final eMed salinity below the Sicily Sill at the end of basin refilling (Zanclean flooding), as a function of initial Mediterranean residual fluid salinity. Residual fluid salinity in wMed and eMed are considered equal. Below 140 PSU, all wMed salt will be transferred to the eMed. **d**, eMed evolving phase when initial residual fluid salinity is set below 140 PSU (140 PSU was used for the main text model calculations - see Methods for reasoning). Duration of salt removal is tested at initial salinities of 60, 80, 100, and 120 PSU. The dotted line represents the maximum eMed surface salinity. The purple box above the time axis represents the expected salt removal duration for salinities between 60 and 120 PSU.

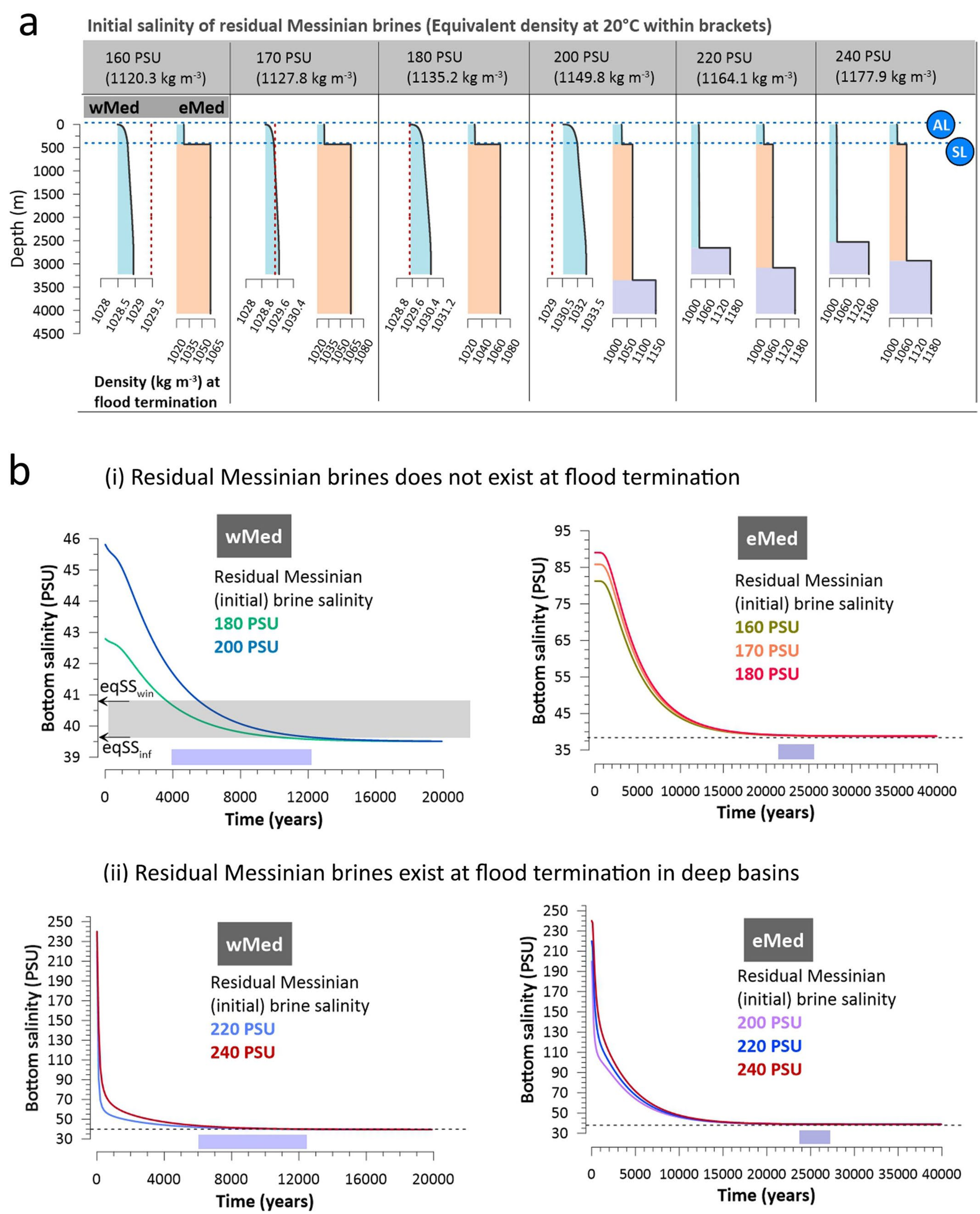

Extended Data Fig. 8 | See next page for caption.

Extended Data Fig. 8 | Summary of sensitivity test (Part 3) results. a, Post-flood density profiles for the wMed and eMed for initial salinities > 140 PSU. Salinities between 160 and 240 PSU were chosen. The vertical dotted line (red) represents the winter density of wMed surface waters. Up to 170 PSU, the post-flood wMed density profile has lower than winter density values. This will result in rapid convective mixing and removal of remaining wMed salt. Above 180 PSU, greater than winter surface densities appear in the wMed. Above 220 PSU, flood energy is no longer sufficient to transfer deep wMed salt to the eMed. Strong eMed stratification is present in all cases (profile shading: blue-green, wMed mixed layer; orange, eMed mixed layer; purple, residual Messinian brines; AL, Atlantic level; SL, Sicily Sill level). **b**, Duration of wMed and eMed salt removal, where stratification exists. The Figure is separated into two parts due to the wide salinity range. For the wMed, model outputs indicate salt removal durations of ~4,000 years at an initial 180 PSU salinity, which can increase up to 12,000 years at 240 PSU. For the eMed, a range between ~21,500 to 27,500 years is expected between 160 and 240 PSU. The purple box above the time axis represents the expected salt removal duration ($eqSS_{win}$, equal surface salinity of winter surface water; $eqSS_{inf}$, equal salinity of inflow water – see Methods for explanation).

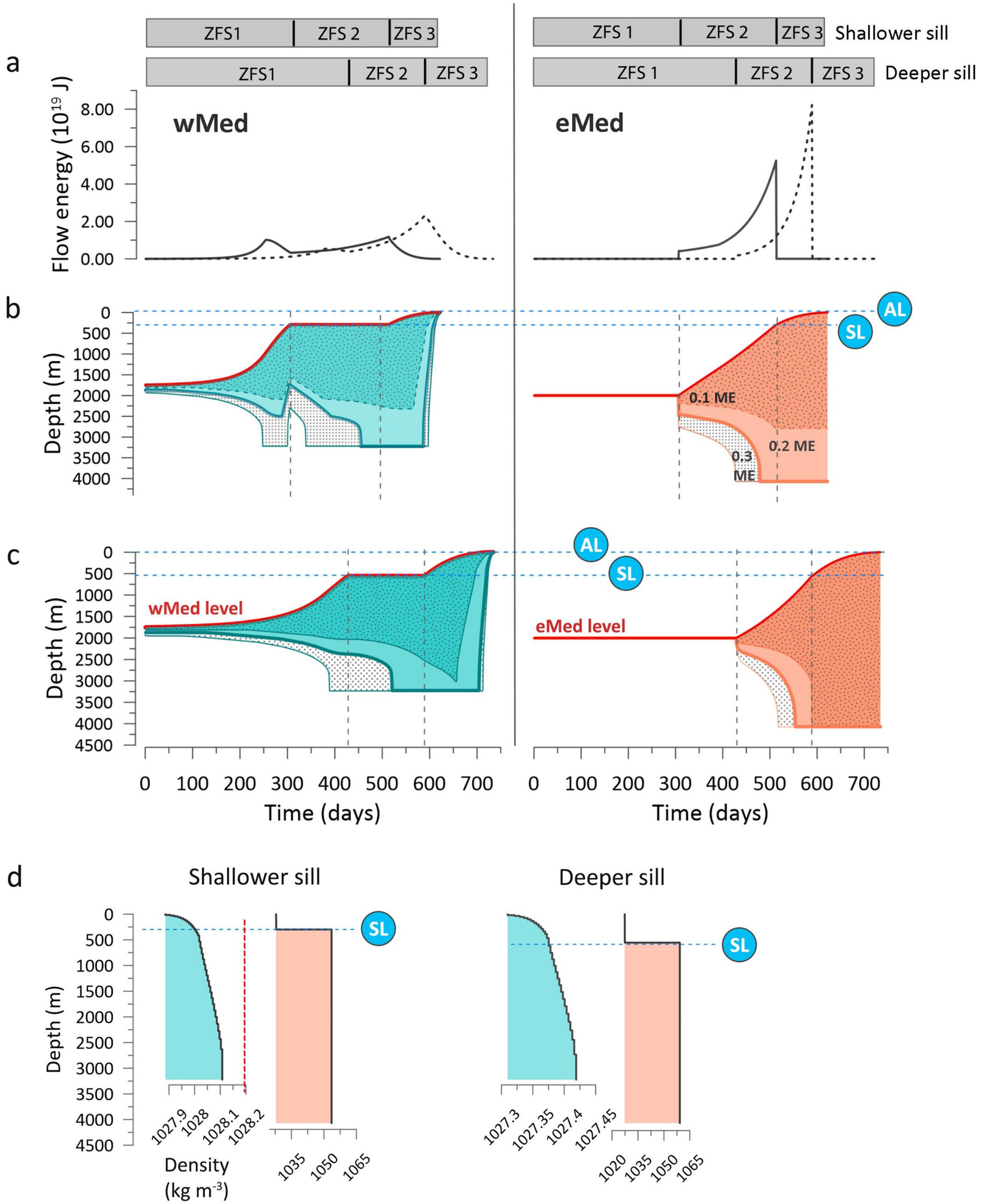

Extended Data Fig. 9 | See next page for caption.

Extended Data Fig. 9 | Summary of sensitivity test (Part 4) results. a, Flow energy in the wMed and the eMed for a ~30% shallower (300 m) or deeper (560 m) than present Sicily sill. Thick and dotted lines correspond to energy evolution for shallow and deep sill depths, respectively. **b**, Sea-level and mixing depth evolution for the wMed and the eMed when the Sicily sill is shallower than present (300 m). **c**, Sea-level and mixing depth evolution for the wMed and the eMed when the Sicily sill is deeper than present (560 m). In b and c, red curves in each panel represent the rise of basin level. Green (for wMed) and orange (for eMed) curves indicate the mixing depth evolution with time, for different mixing efficiencies (ME). Dots in coloured background, 0.1 ME; coloured-only background, 0.2 ME; Dots in white background, 0.3 ME. For a, b and c, refer to the grey colour panels at the top of the figure for Zanclean flooding stages (ZFS 1–3) for shallower and deeper sill settings. **d**, Density profiles at the end of the flooding phase for shallow and deep sill settings. Vertical red-dotted line represents the present wMed surface density (Mediterranean Atlantic water density in the wMed[29]). Green shading, wMed mixed layer; orange shading, eMed mixed layer; AL, Atlantic level; SL, Sicily sill level.

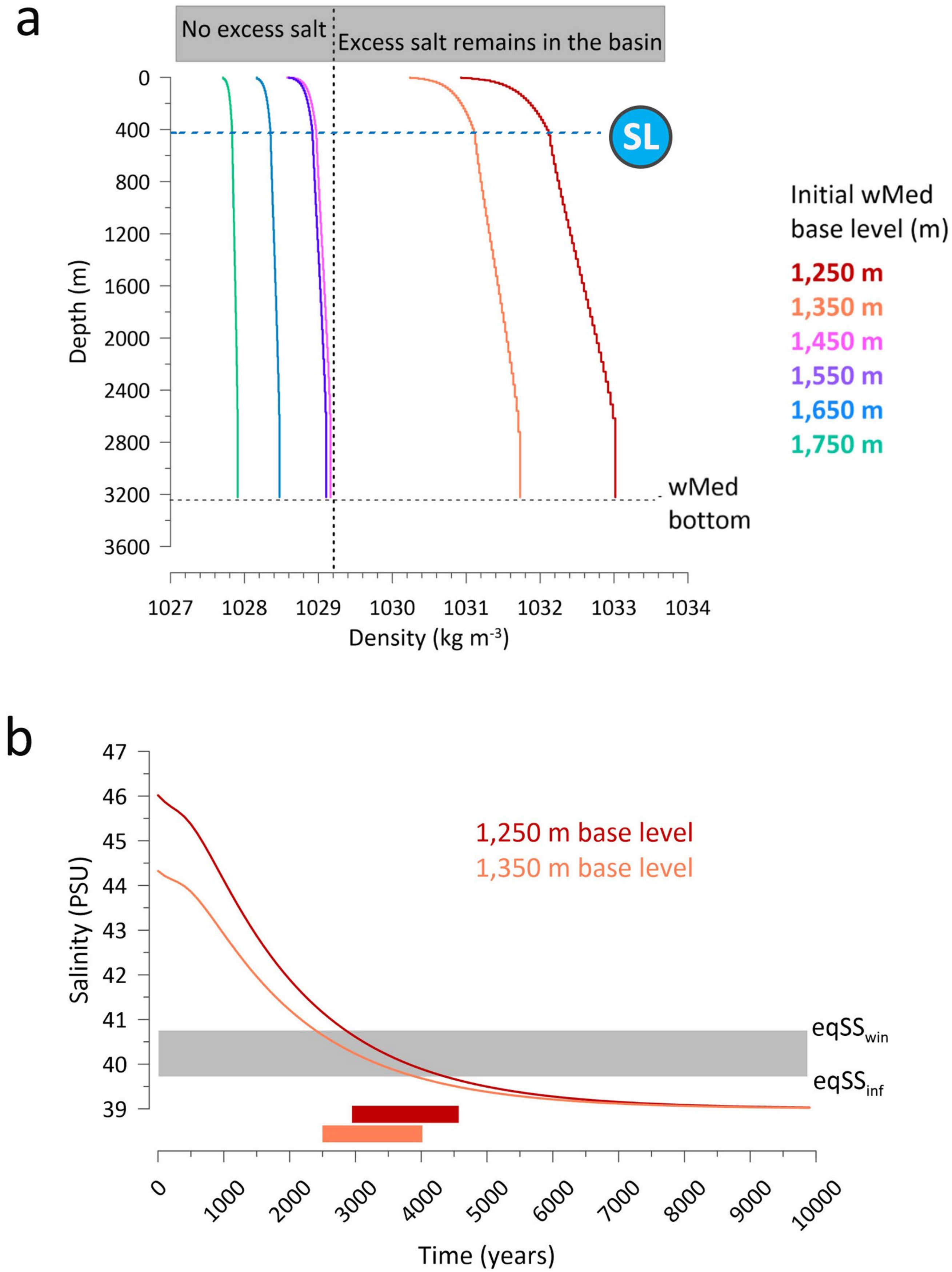

Extended Data Fig. 10 | See next page for caption.

Extended Data Fig. 10 | Summary of sensitivity test (Part 5) results. a, Density profiles for the wMed at the flooding phase termination, for different starting base levels of the wMed and the eMed (eMed base level is 250 m lower than the mentioned wMed base level for each test). Vertical dotted line represents the winter wMed surface density. Beyond this line, excess salt remains in the wMed as a result of incomplete salt transfer to the eMed. **b**, Duration of post-flood salt diffusion for starting base levels which results in excess salt in the wMed (1,250 and 1,350 m wMed base levels below Atlantic level; correspond to 1,500 and 1,600 eMed levels, respectively). Coloured panels above the time axis represent the expected duration of salt removal from wMed to the Atlantic, for corresponding curves with same colour ($eqSS_{win}$, equal surface salinity of winter surface water; $eqSS_{inf}$, equal salinity of inflow water – see Methods for explanation). SL; Sicily sill level.